Hindawi
Computational and Mathematical Methods in Medicine
Volume 2022, Article ID 1715414, 25 pages
https://doi.org/10.1155/2022/1715414

Research Article

A Mathematical Evaluation of the Cost-Effectiveness of Self-Protection, Vaccination, and Disinfectant Spraying for COVID-19 Control

Sacrifice Nana-Kyere[1,2] **and Baba Seidu**[1]

[1]*Department of Mathematics, C. K. Tedam University of Technology and Applied Sciences, Navrongo, Ghana*
[2]*Department of Mathematics and Information Technology, Valley View University, Ghana*

Correspondence should be addressed to Baba Seidu; bseidu@cktutas.edu.gh

Received 3 July 2022; Revised 31 August 2022; Accepted 18 November 2022; Published 29 December 2022

Academic Editor: Shahzad Sarwar

The world is on its path from the post-COVID period, but a fresh wave of the coronavirus infection engulfing most European countries makes the pandemic catastrophic. Mathematical models are of significant importance in unveiling strategies that could stem the spread of the disease. In this paper, a deterministic mathematical model of COVID-19 is studied to characterize a range of feasible control strategies to mitigate the disease. We carried out an analytical investigation of the model's dynamic behaviour at its equilibria and observed that the disease-free equilibrium is globally asymptotically stable when the basic reproduction number, $\mathscr{R}_0$ is less than unity. The endemic equilibrium is also shown to be globally asymptotically stable when $\mathscr{R}_0 > 1$. Further, we showed that the model exhibits forward bifurcation around $\mathscr{R}_0 = 1$. Sensitivity analysis was carried out to determine the impact of various factors on the basic reproduction number $\mathscr{R}_0$ and consequently, the spread of the disease. An optimal control problem was formulated from the sensitivity analysis. Cost-effectiveness analysis is conducted to determine the most cost-effective strategy that can be adopted to control the spread of COVID-19. The investigation revealed that combining self-protection and environmental control is the most cost-effective control strategy among the enlisted strategies.

1. Introduction

The world is on its path from the post-COVID fiscal year. However, a fresh wave of the coronavirus infection engulfing the European countries makes the pandemic catastrophic, with most regions grappling with their worst outbreaks since the pandemic began [1]. Since December 2019, when the coronavirus epidemic was reported in Hubei in China, the epidemic has threatened the global well-being of humans by significantly affecting human resources through sickness and death [2]. Asian countries such as India, Sri Lanka, and Thailand are battling COVID-19 containment. The rapid resurgence of the virus has put enormous pressure on these countries' health systems and medical supplies, with some calling for foreign assistance amid the escalating crisis. Generally, the availability of vaccines and the introduction of various vaccination programs have lowered the global daily infection and death counts, yet the deaths and infections have not entirely abated [3]. Mathematical models have made an indelible mark on the fight against infectious diseases by identifying protocols to respond to hikes in the transmission dynamics of epidemics [4–12]. Notable works in the case of COVID-19 have been considered by several authors. Yang et al. [13] made a generalized prediction of the coronavirus epidemic in mainland China by considering an SEIR model that utilized the available data. Zuo et al. [14] presented a data analysis and comparison method that concerned institutions could employ for proper decision making.calibrated the Brazil coronavirus

pandemic that worked on determining the peak time of the epidemic. Wu et al. [2] used the available data from China to establish the possibility of symptomatic people dying from the coronavirus epidemic. Götz and Heidrich [15] considered a mathematical model of the COVID-19 epidemic that used data from Germany to estimate the model's parameters and established the ascertainment of official infected cases. In [16], a nonlinear coronavirus model was considered and utilized to fit China's data to estimate the model's parameters. Abbasi et al. developed a mathematical model for the novel coronavirus disease and proved through stability analysis studies that, mitigating measures alone could not eradicate the disease. Their conclusion was based on the fact that the endemic equilibrium was globally asymptotically stable. Gu et al. [17] proposed a mathematical model that primarily focused on isolation, quarantine, and hospitalization to study the transmission dynamics of the novel coronavirus epidemic. They exploited nonpharmaceutical intervention measures: social distancing, isolation, contact tracing, and quarantine to mitigate the spreading of the disease. The authors further rebuilt the model into a stochastic model and compared the stochastic model analysis to the deterministic one. Currie et al. [18] developed a mathematical COVID-19 model that identified how mathematical models could influence management decision-making. In a related study, Huang et al. [19] constructed a mathematical model with several compartments that calibrated the model's parameters with the available data and predicted the transmissibility of COVID-19. Senapati et al. [20] designed a nonlinear model that considered India's data to estimate the model's parameters and established the effectiveness of various protocols ushered in to suppress the disease. Zhou et al. [21] considered a SEIR COVID-19 model and applied the available data to estimate the reproduction number. In [22], a SEIR model was calibrated to the available data to derive some vital model parameters and determine the propagation trend of the epidemic. Hou et al. [23] proposed a nonlinear SEIR compartmental model that assessed the potency of Wuhan's quarantine measure during the peaks of the epidemic and estimated the model's parameters by fitting the model to Wuhan's data. The model proposed by Du and Yuan [24] examined the propagation trend of the SARS-CoV2 and validated the model with existing Influenza data. Petropoulos and Makridakis [25] made a generalized prediction of the SARS-CoV2 pandemic pattern in Cyprus and underlaid strategies for containing the epidemic.

Optimal control models have received credit from the scientific community for their contribution in determining essential measures for pushing down cases of infections and the spike of new variants [26–33]. In December 2019, when WHO ascertained the existence of the pandemic, intriguing optimal control studies have been carried out that helped to wrestle the epidemic from spreading. Nana-Kyere et al. [34] presented a coronavirus model that mainly examined the epidemic's stability and constructed an optimal control problem to deduce potent strategies to curb the disease. Asamoah et al. [35] calibrated their model to Ghana's data to estimate some essential parameters that influence the dynamics of the disease. They extended the model to an optimal control problem to pinpoint strategies that will boost lowering the infected cases of the pandemic with minimal cost. Tsay et al. [36] studied the dynamical behaviour of the epidemic by designing a compartmental model for the disease. They redesigned the model into the optimal control problem to find strategies to help manage the virus. Kouidere et al. [37] characterized some feasible control strategies that come with desirable impact in containing the 2019 coronavirus epidemic. Perkins and Guido [38] considered an unorthodox method of handling epidemic without involving drugs to determine how the coronavirus infection could be managed. They reformulated the model into an optimal control problem to deduce strategies paramount for curtailing the disease. A nonlinear COVID-2019 model was developed to calibrate the model's parameters by fitting the model to Ethiopia's data [39]. The mode was extended into an optimal control problem in order to determine the effectiveness of treatment controls, personal protection, and public health education's in suppressing the epidemic. Srivastav et al. [40] categorized a compartmental COVID-19 model into two main groups of the aged and young and used the data of Italy and Spain to estimate some of the model's parameters. The authors then considered optimal control methods that developed strategies for managing the epidemic. Seidu [41] proposed a SARS-CoV2 mathematical model that captured the respective roles of mildly symptomatic, severely symptomatic, and exposed individuals in the transmission of the disease. He modified the model to optimal control and determined the most cost-effective strategy among the considered strategies through the cost-effectiveness method. In another related study, Nana-Kyere et al. [42] proposed a nonlinear mathematical model for the COVID-19 virus that examined the transmission dynamics of the disease. They modified the model into an optimal control problem and solved it to determine whether the proposed control strategies were potent enough to mitigate the epidemic from spreading. Agossou et al. [43] assessed the effects of pharmaceutical and nonpharmaceutical control strategies on the transmission dynamics of the COVID-19 epidemic.

The COVID-19 epidemic has attracted a voluminous amount of information from mathematical models since the time the disease was confirmed by WHO. Nevertheless, a significant amount of these pieces of information cannot be adequately relied on by public health to contain the virus. The unreliability of these models is because they are not epidemiologically well-composed and do not accurately describe the propagation trends of the disease for the correct management decision to be taken. This research mainly focuses on extending the model of Khan et al. [44] into an optimal control problem by identifying control strategies for the COVID epidemic and carrying out a socioeconomic analysis of the identified strategies to boost management decision-making on the containment of the virus. This has become necessary as the control model analysis would

provide policy direction for public health. The paper will add to the existing knowledge on the epidemic dynamics by assessing the combined effect of treatment, vaccination, and disinfection of the environment on the transmission dynamics of the disease.

The rest of the research is presented as follows: Section 2 "The Model Development" presents the model formulation, model's parameter definition, invariant region, boundedness, and stationary points. Section 3 "Qualitative Analysis" deals with the stability analysis, sensitivity and bifurcation analysis. In Section 4 "Development of Optimal Control Model", we present an optimal control problem formulation and its qualitative analysis. Section 5 "Numerical Experimentation and Discussion" provides the numerical solution for the models. In Section 6 "Economic Cost Analysis of the Control Implementation", a cost-effectiveness analysis is carried out to determine the most cost-effective strategy among the considered strategies. The section also discusses the simulated results of the work with a recommended conclusion.

2. The Model Development

The aggressiveness of the COVID-19 disease on the population means that newly designed models need to identify measures that would help clamp down on the disease. In this research, we use the COVID-19 model studied by Khan et al. [44]. The work segregates the model into eight compartments of Susceptible S, Exposed E, Infected I, asymptomatically infected A, Quarantined Q , Hospitalized H, Recovered R, and virus concentration in the environment M. The model assumes that Susceptible individuals are recruited into the population at a rate of Λ persons per unit time. The contact between a naive susceptible individual on the one hand and the infected or the asymptomatically infected on the other hand is given by η_1. The parameter ψ represents the transmissibility factor associated with the Asymptomatically infected persons. The model assumes that, the mortality that occurs naturally in individuals is given by μ. The parameter θ denotes the infection following exposure. The parameters ω and ρ are the incubation periods of the disease. The infected, asymptomatically infected, quarantined, and hospitalized individuals have recovery rates, respectively, given by $\tau_1, \tau_2, \phi_1, \phi_2$. The infected and quarantined individuals are hospitalized at rates γ and δ_2. The COVID-19-induced death rates in the infected and hospitalized are ξ_1 and ξ_2. Susceptible individuals contract the disease at a rate η_2 due to a visit to the seafood market and contacting a viral source there or eating from a Covid-19-infected animal. The model assumes that the infected and asymptomatically infected individuals contribute to viral deposits in the seafood market at rate q_1 and q_2, respectively. The parameter q_3 denotes the rate of removal of coronaviruses from the seafood market. Finally, the exposed individuals are quarantined at a rate δ_1. Based on these assumptions, the proposed dynamical COVID-19 model is of the form:

$$\left.\begin{aligned}
\frac{dS}{dt} &= \Lambda - \mu S - \eta_2 MS - \eta_1 \frac{\mathrm{IS}}{N} - \frac{\psi AS}{N}\eta_1,\\
\frac{dE}{dt} &= \eta_2 MS + \eta_1 \frac{\mathrm{IS}}{N} + \frac{\psi AS}{N}\eta_1 - ((1-\theta)\omega + \theta\rho + \delta_1 + \mu)E,\\
\frac{dI}{\mathrm{d}t} &= (1-\theta)\omega E - (\tau_1 + \xi_1 + \gamma + \mu)I,\\
\frac{dA}{dt} &= \theta\rho E - (\tau_2 + \mu)A,\\
\frac{dQ}{dt} &= \delta_1 E - (\phi_1 + \delta_2 + \mu)Q,\\
\frac{dH}{dt} &= \gamma I + \delta_2 Q - (\phi_2 + \xi_2 + \mu)H,\\
\frac{dR}{dt} &= \tau_1 I + \tau_2 A + \phi_1 Q + \phi_2 H - \mu R,\\
\frac{dM}{dt} &= q_1 I + q_2 A - q_3 M,\\
&\text{with } S(0) \geq 0, E(0) \geq 0, I(0) \geq 0, A(0) \geq 0, Q(0) \geq 0,\\
&\quad H(0) \geq 0, R(0) \geq 0 \text{ and } M(0) \geq 0.
\end{aligned}\right\} \tag{1}$$

2.1. Qualitative Analysis: Disease-Free Equilibrium and the $\mathscr{R}_0$. In an epidemiological setting, the basic reproduction number $\mathscr{R}_0$, crystallizes the ability of the infection to spread or die out in the population. The $\mathscr{R}_0$ is a measure of the number of people, on average, each sick person will infect throughout its period of infectivity. When $\mathscr{R}_0$ is above one, the epidemic is generally recognized to be growing, and when the number is less than one, the outbreak is said to be declining. According to Khan et al. [44], $\mathscr{R}_0$, the basic reproduction number is given by

$$\mathscr{R}_0 = \frac{\eta_2\Lambda(1-\theta)\omega q_1}{\mu q_3 R_1 R_2} + \frac{\theta\rho\eta_2\Lambda q_2}{\mu q_3 R_1 R_3} + \frac{\psi\eta_1\theta\rho}{R_1 R_3} + \frac{\eta_1(1-\theta)\omega}{R_1 R_2}, \tag{2}$$

where

$$R_1 = ((1-\theta)\omega + \theta\rho + \delta_1 + \mu), R_2 = (\tau_1 + \xi_1 + \gamma + \mu), R_3 = (\tau_2 + \mu). \tag{3}$$

2.2. Endemic Equilibrium. Any system that is not characterized by an absence of infection but rather a high transmissibility rate will eventually result in an endemic state. The model Equation (1) has a unique endemic equilibrium given as

$$\left.\begin{aligned}
S^* &= \frac{\Lambda}{\mathscr{R}_0},\\
Q^* &= \frac{\delta_1 E^*}{(\phi_1 + \delta_2 + \mu)},\\
A^* &= \theta\rho E^*,\\
I^* &= (1-\theta)\omega E^*,\\
M^* &= \frac{q_1 I^* + q_2 A^*}{q_3},\\
H^* &= \frac{\gamma I^* + \delta_2 Q^*}{\phi_2 + \xi_2 + \mu},\\
R^* &= \frac{\tau_1 I^* + \tau_2 A^* + \phi_1 Q^* + \phi_2 H^*}{\mu},\\
E^* &= \frac{\Lambda q_3(\Lambda\mathscr{R}_0 + \mu)(\tau_1 + \xi_1 + \gamma + \mu)(\tau_2 + \mu)}{\mu(\eta_2 q_1 g_1 + \eta_2 q_2 g_2 + \eta_1 q_3 g_3 + \eta_1\psi g_4)},
\end{aligned}\right\} \tag{4}$$

with $g_1 = N(1-\theta)\omega(\tau_2+\mu)$, $g_2 = N\theta\rho(\tau_1+\xi_1+\gamma+\mu)$, $g_3 = (1-\theta)\omega(\tau_2+\mu)$, and $g_4 = \theta\rho(\tau_1+\xi_1+\gamma+\mu)$.

Using the analysis from [44] with the notation $\lambda = \eta_2 MS + \eta_1(\mathrm{IS}/N) + (\psi AS/N)\eta_1$. the endemic equilibrium can be characterised in terms of $\mathscr{R}_0$ as

$$F(\lambda^{**}) = l_1(\lambda^{**})^2 + l_2\lambda^{**} + l_3, \tag{5}$$

where

$$\begin{aligned}
l_1 &= k_1k_2k_3q_3(k_3(\delta_1k_2(\delta_2(\mu+\phi_2)+k_5(\mu+\phi_1))+k_4k_6)+\theta k_2k_4k_5\rho(\mu+\tau_2)),\\
l_2 &= k_1k_2k_3\mu q_3(k_3(\delta_1k_2(\delta_2(\mu+\phi_2)+k_5(\mu+\phi_1))+k_4k_8)+\theta k_2k_4k_5\rho(-\eta_1\psi+\mu+\tau_2))\\
&\quad+\eta_2k_7\Lambda((1-\theta)k_3q_1\omega-\theta k_2\rho q_2)+k_1^2k_2^2k_4k_5k_3^2\mu q_3,\\
l_3 &= k_1^2k_2^2k_3^2k_4k_5\mu^2q_3(1-\mathscr{R}_0),\\
k_1 &= \delta_1+\theta\rho+(1-\theta)\omega+\mu,\ k_2=\gamma+\mu+\xi_1+\tau_1,\ k_3=\mu+\tau_2,\\
k_4 &= \delta_2+\mu+\phi_1,\ k_5=\mu+\xi_2+\phi_2,\\
k_6 &= \gamma(1-\theta)\omega(\mu+\phi_2)+k_5((1-\theta)\omega(\mu+\tau_1)+k_2\mu),\\
k_7 &= k_3(-\delta_1k_2(\delta_2(\mu+\phi_2)+k_5(\mu+\phi_1))-k_4k_6)-\theta k_2k_4k_5\rho(\mu+\tau_2),\\
k_8 &= \gamma(1-\theta)\omega(\mu+\phi_2)+k_5((1-\theta)\omega(-\eta_1+\mu+\tau_1)+k_2\mu).
\end{aligned} \tag{6}$$

The Equation (5) is used to generate the bifurcation plot in Figure 1, which was not done in [44].

3. Qualitative Analysis: Global Stability-Disease Free Equilibrium

In performing the global qualitative analysis, we employed the method of Castillo-Chavez et al. [45] to investigate the global stability of the state Equation (1) at the disease-free equilibrium. Following Castillo-Chavez et al. [45], the COVID-19 model Equation (1) can be restructured as follows:

$$\begin{aligned}
\frac{dy_1}{dt} &= W_1(y_1,y_2),\\
\frac{dy_2}{dt} &= W_2(y_1,y_2),\ W_2(y_1,0)=0,
\end{aligned} \tag{7}$$

with $y_1 = (S,R)$ representing the uninfected population, and $y_2 = (E,I,A,Q,H,M)$ denoting the infected. The disease-free equilibrium point is given by.

If the following criteria are satisfied, the point $U_1 = (y_1^0, 0)$ is a globally asymptotically stable equilibrium for the model (1).

F1: Given $dy_1/dt = W_1(y_1,0)$, (y_1^0) is globally asymptotically stable.

F2: $W(y_1,y_2) = Dy_2 - \tilde{W}_2(y_1,y_2)$, where $\tilde{W}_2(y_1,y_2) \geq 0$ for $(y_1,y_2) \in \zeta$.

Theorem 1. *The point $U_1 = (y_1^0, 0)$ is globally asymptotically stable equilibrium whenever $\mathscr{R}_0 < 1$.*

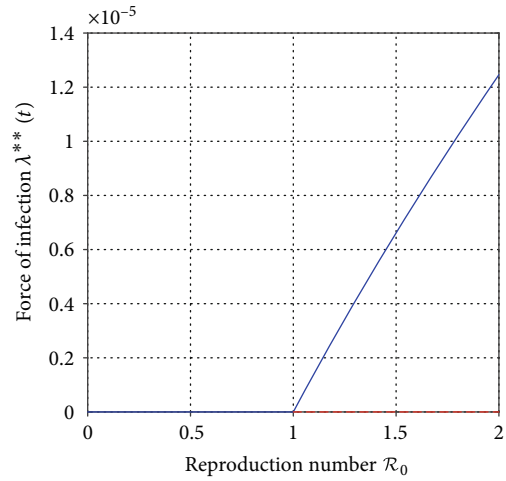

Figure 1: Forward bifurcation diagram.

Proof. Considering the model Equation (1), we generate $W_1(y_1,y_2)$ and $W_2(y_1,y_2)$ as;

$$\begin{aligned}
W_1(y_1,y_2) &= \begin{pmatrix} \Lambda-\mu S-\eta_2MS-\eta_1\dfrac{\mathrm{IS}}{N}-\dfrac{\psi AS}{N}\eta_1 \\ \tau_1I+\tau_2A+\phi_1Q+\phi_2H-\mu R \end{pmatrix},\\
W_2(y_1,y_2) &= \begin{pmatrix} \eta_2MS+\eta_1\dfrac{\mathrm{IS}}{N}+\dfrac{\psi AS}{N}\eta_1-((1-\theta)\omega+\theta\rho+\delta_1+\mu)E \\ (1-\theta)\omega E-(\tau_1+\xi_1+\gamma+\mu)I \\ \theta\rho E-(\tau_2+\mu)A \\ \delta_1E-(\phi_1+\delta_2+\mu)Q \\ \gamma I+\delta_2Q-(\phi_2+\xi_2+\mu)H \\ q_1I+q_2A-q_3M \end{pmatrix}.
\end{aligned} \tag{8}$$

With $S = S_0$, $I = I_0$, $A = A_0$, $R = R_0$ and $M = M_0$ then $W_1(y_1,0)$ becomes

$$W_1(y_1,y_2) = \begin{pmatrix} \Lambda-\mu S_0-\eta_2M_0S_0-\eta_1\dfrac{I_0S_0}{N}-\dfrac{\psi A_0S_0}{N}\eta_1 \\ \tau_1I_0+\tau_2A_0+\phi_1Q_0+\phi_2H_0-\mu\mathscr{R}_0 \end{pmatrix}. \tag{9}$$

It can be shown from (9) that as $t \longrightarrow \infty$, $y_1 \longrightarrow y_1^0$. Hence $y_1 = y_1^0$ is globally asymptotically stable, which satisfies condition one. Now, ascertaining whether condition (F_2) would be satisfied, we consider $W(y_1,y_2) = Dy_2 - \tilde{W}_2(y_1,y_2)$. Thus, we have

$$W_1(y_1,y_2) = \begin{pmatrix} -k_1 & \dfrac{\eta_1}{N}S_0 & \dfrac{\psi\eta_1}{N}S_0 & 0 & 0 & \eta_2S_0 \\ (1-\theta)\omega & -k_2 & 0 & 0 & 0 & 0 \\ \theta\rho & 0 & -k_3 & 0 & 0 & 0 \\ \delta_1 & 0 & 0 & -k_4 & 0 & 0 \\ 0 & \gamma & 0 & \delta_2 & -k_5 & 0 \\ 0 & q_1 & q_2 & 0 & 0 & -q_3 \end{pmatrix} \begin{pmatrix} E \\ I \\ A \\ Q \\ H \\ M \end{pmatrix} - \begin{pmatrix} \tilde{W}_2(y_1,y_2) \\ 0 \\ 0 \\ 0 \\ 0 \\ 0 \end{pmatrix}, \tag{10}$$

where matrix D given by

$$D = \begin{pmatrix} -k_1 & \frac{\eta_1}{N}S_0 & \frac{\psi\eta_1}{N}S_0 & 0 & 0 & \eta_2 S_0 \\ (1-\theta)\omega & -k_2 & 0 & 0 & 0 & 0 \\ \theta\rho & 0 & -k_3 & 0 & 0 & 0 \\ \delta_1 & 0 & 0 & -k_4 & 0 & 0 \\ 0 & \gamma & 0 & \delta_2 & -k_5 & 0 \\ 0 & q_1 & q_2 & 0 & 0 & -k_{66} \end{pmatrix} \text{ with } \tilde{W}_2(y_1, y_2)$$
$$= (S_0 - S)\begin{pmatrix} \eta_2 M & \frac{\eta_1 I}{N} & \frac{\psi\eta_1 A}{N} \\ 0 & 0 & 0 \\ 0 & 0 & 0 \\ 0 & 0 & 0 \\ 0 & 0 & 0 \\ 0 & 0 & 0 \end{pmatrix}, \tag{11}$$

It can be deduced from model Equation (1) that the total population is bounded by S_0. Hence, $\eta_2 MS \le \eta_2 MS_0$, $(\eta_1 I/N)S \le (\eta_1 I/N)S_0$ and $(\psi\eta_1 A/N)S \le (\psi\eta_1 A/N)S_0$ which implies $\tilde{W}_2(y_1, y_2)$ is positive definite. Additionally, matrix D is undoubtedly an M-matrix, with the off-diagonal entries positive. Hence, the requirement of the two conditions is met, proving the global asymptotic stability of U_1. □

3.1. Qualitative Analysis: Global Stability-Endemic Equilibrium. In assessing global asymptotic stability of the endemic equilibrium of the model system (1), we capitalize on the geometrical method [46] which uses Bendixson criterion as sufficient condition for determining model system (1) global stability.

Theorem 2. *Given $\mathcal{R}_0 > 1$, the endemic equilibrium of model Equation (1) is globally asymptotically stable; otherwise, it is unstable.*

Proof. In proving the global stability of the endemic equilibrium, the study of ([47], with referencing to Lemma 3, Lemma 4 and Theorem 5.) is considered. we consider the subsystem of model Equation (1) as

$$\begin{cases} \frac{d}{dt}S = \Lambda - \mu S - \eta_2 MS - \eta_1 \frac{\mathrm{IS}}{N} - \frac{\psi AS}{N}\eta_1, \\ \frac{d}{dt}E = \eta_2 MS + \eta_1 \frac{\mathrm{IS}}{N} + \frac{\psi AS}{N}\eta_1 - ((1-\theta)\omega + \theta\rho + \delta_1 + \mu)E, \\ \frac{d}{dt}I = (1-\theta)\omega E - (\tau_1 + \xi_1 + \gamma + \mu)I. \end{cases} \tag{12}$$

Considering subsystem (12) the Jacobian matrix becomes,

$$J_v = \begin{pmatrix} -w_{11} & 0 & -\eta_1 S/N \\ w_{21} & -w_{22} & \eta_1 S/N \\ 0 & (1-\theta)\omega & -w_{33} \end{pmatrix}, \tag{13}$$

with

$$w_{11} = \Lambda - \eta_2 M - \eta_1 \frac{I}{N} - \frac{\psi A}{N}\eta_1 - \mu, \quad w_{21} = \eta_2 M - \eta_1 \frac{I}{N} - \frac{\psi A}{N}\eta_1,$$
$$w_{22} = -((1-\theta)\omega + \theta\rho + \delta_1 + \mu), \qquad w_{33} = -(\tau_1 + \xi_1 + \gamma + \mu). \tag{14}$$

Then, $J_v^{|2|}$, the second additive matrix of J_v is given by

$$J_v^{|2|} = \begin{pmatrix} -(w_{11} + w_{22}) & \frac{\eta_1 S}{N} & -\frac{\eta_1 S}{N} \\ ((1-\theta)\omega) & -(w_{11} + w_{33}) & 0 \\ 0 & \eta_2 M - \eta_1 \frac{I}{N} - \frac{\psi A}{N}\eta_1 & -(w_{22} + w_{33}) \end{pmatrix}. \tag{15}$$

Now, we denote the function $P(y) = P(S, E, I) = \mathrm{diag}\{1, (E/I), (E/I)\}$, hence we deduce $P^{-'}(y) = \mathrm{diag}\{1, (I/E), (I/E)\}$. Then, the time derivative of $P_f(y)$ becomes $P_f(y) = \mathrm{diag}\{0, \tilde{E}/I - E\tilde{I}/I^2, \tilde{E}/I - E\tilde{I}/I^2\}$ and $P_f(y)P^{-'}(y) = \mathrm{diag}\{0, \tilde{E}/E - \tilde{I}/I, \tilde{E}/E - \tilde{I}/I\}$. It follows that

$$P_f(y)J_v^{|2|}P^{-'}(y)\Big) = \begin{pmatrix} -(w_{11} + w_{22}) & \frac{\eta_1 SI}{NE} & -\frac{\eta_1 SI}{NE} \\ \frac{((1-\theta)\omega E)}{I} & -(w_{11} + w_{33}) & 0 \\ 0 & \eta_2 M - \eta_1 \frac{I}{N} - \frac{\psi A}{N}\eta_1 & -(w_{22} + w_{33}) \end{pmatrix}. \tag{16}$$

Hence, matrix $C = P_f(y)J_v^{|2|}P^{-'}(y)) + P_f(y)P^{-'}(y)$ can be determined and written as;

$$C = \begin{pmatrix} C_{11} & C_{12} \\ C_{21} & C_{22} \end{pmatrix}, \tag{17}$$

where

$$C_{11} = -\eta_2 M - \eta_1 \frac{I}{N} - \frac{\psi A}{N}\eta_1 - \mu - ((1-\theta)\omega + \theta\rho + \delta_1) - 2\mu, C_{12} = \left(\frac{\eta_1 SI}{NE}, -\frac{\eta_1 SI}{NE}\right),$$

$$C_{21} = \left(\frac{((1-\theta)\omega E)}{I}, 0\right) \text{ and}$$

$$C_{22} = \begin{pmatrix} w_2 + \frac{\tilde{E}}{E} - \frac{\tilde{I}}{I} & 0 \\ \eta_2 M - \eta_1 \frac{I}{N} - \frac{\psi A}{N}\eta_1 & w_3 + \frac{\tilde{E}}{E} - \frac{\tilde{I}}{I} \end{pmatrix}, \tag{18}$$

with

$$\begin{cases} w_2 = -\eta_2 M - \eta_1 \dfrac{I}{N} - \dfrac{\psi A}{N}\eta_1 - (\tau_1 + \xi_1 + \gamma) - 2\mu, \\ w_3 = -((1-\theta)\omega + \theta\rho + \delta_1 + \mu) - (\tau_1 + \xi_1 + \gamma) - 2\mu. \end{cases} \tag{19}$$

Consider (n_1, n_2, n_3) to be a vector in $\mathbb{R}^3$ and the norm $(\|\bullet\|)$ given by $(\|n_1, n_2, n_3\|) = \max\{|n_1|, |n_2|, |n_3|\}$. Let $\rho_1(C)$ represents the Lozinki measure with respect to this norm; we adopt the method of approximating the $\rho_1(C)$ as explored in [48], and choose $\rho_1(C) \le \sup\{p_1, p_2\}$, where $\sup\{p_1, p_2\} = \{\rho_1(C_{11}) + |C_{12}|, \rho_1(C_{22}) + |C_{21}|\}$ and $|C_{12}|$ and $|C_{21}|$ are matrix norms with respect to vector norms ρ_1, and ρ represents the Lozinki measure with respect to the norm ρ_1.

Then, $\rho_1(C_{11}) = -\eta_2 MS - \eta_1(I/N)S - (\psi AS/N)\eta_1 - \mu - ((1-\theta)\omega + \theta\rho + \delta_1) - 2\mu$

$$\begin{aligned} |C_{12}| &= \max\left\{\frac{\eta_1 S}{NE}, -\frac{\eta_1 S}{NE}\right\} = \frac{\eta_1 SI}{NE}, \\ |C_{12}| &= \max\left\{\frac{((1-\theta)\omega E)}{I}, 0\right\} = \frac{((1-\theta)\omega E)}{I}, \\ \rho_1(C_{22}) &= \frac{\tilde{E}}{E} - \frac{\tilde{I}}{I} - (\tau_1 + \xi_1 + \gamma) - 2\mu. \end{aligned} \tag{20}$$

Hence,

$$\begin{aligned} p_1 &= -\eta_2 MS - \eta_1 \frac{I}{N} S - \frac{\psi AS}{N}\eta_1 - ((1-\theta)\omega + \theta\rho + \delta_1) - 2\mu + \frac{\eta_1 SI}{NE}, \\ p_2 &= -\frac{\tilde{E}}{E} - \frac{\tilde{I}}{I} - (\tau_1 + \xi_1 + \gamma) - 2\mu + \frac{(1-\theta)\omega E}{I}. \end{aligned} \tag{21}$$

It could be verified that

$$\begin{aligned} \frac{\tilde{E}}{E} &= \frac{\eta_2 MS}{E} + \eta_1 \frac{\mathrm{IS}}{NE} + \frac{\psi AS}{NE}\eta_1 - ((1-\theta)\omega + \theta\rho + \delta_1 + \mu), \\ \frac{\tilde{I}}{I} &= \frac{((1-\theta)\omega E)}{I} - (\tau_1 + \xi_1 + \gamma + \mu), \end{aligned} \tag{22}$$

which provides the following inequalities when substituted into P_1 and P_2 :$P_1 \le (\eta_1 SI/NE) + (\tilde{E}/E) - \mu, P_2 \le \tilde{E}/E - \mu$.

Further,

$$\begin{aligned} \rho_1(C) \le \sup\{p_1, p_2\} &\le \sup\left\{\frac{\eta_1 SI}{NE} + \frac{\tilde{E}}{E} - \mu, \frac{\tilde{E}}{E} - \mu\right\}, \\ &= \frac{\tilde{E}}{E} - \mu + Sup\left\{\frac{\eta_1 SI}{NE}, 0\right\}, = \frac{\tilde{E}}{E} - \mu + \frac{\eta_1 SI}{NE}. \end{aligned} \tag{23}$$

Hence,

$$\rho_1(C) \le \frac{\tilde{E}}{E} - \mu + \frac{\eta_1 SI}{NE}, \tag{24}$$

substitute (24) into the below equation

$$\tilde{q}_a = \lim_{t \longrightarrow \infty} \sup \frac{1}{t}\int_0^t \rho_1(C)dt. \tag{25}$$

Now from Equation (25), we denote $\lambda_1 = \mu$ and $\lambda_2 = \eta_1 SI/NE$, then if $\lambda_2 < \lambda_1$, it follows that $\rho_1(C) \le \tilde{E}/E - \epsilon$ where $\epsilon = \mu - \eta_1 SI/NE$. Now, for $t > T$, it follows that

$$\tilde{q}_a = \lim_{t \longrightarrow \infty} \sup \frac{1}{t}\int_0^t \rho_1(C)dt < -\epsilon < 0. \tag{26}$$

Therefore, from (26), we get $\tilde{q}_a = \lim_{t \longrightarrow \infty} \sup (1/t)\int_0^t \rho_1(C)\, dt < 0$. This verifies that the system of nonlinear differential equation of submodel (12) is GAS around the interior equilibrium of S^*, E^*, I^*. Therefore, considering the remaining subsystem of model (1).

$$\begin{cases} \dfrac{d}{dt}A = \theta\rho E - (\tau_2 + \mu)A, \\ \dfrac{d}{dt}Q = \delta_1 E - (\phi_1 + \delta_2 + \mu)Q, \\ \dfrac{d}{dt}H = \gamma I + \delta_2 Q - (\phi_2 + \xi_2 + \mu)H, \\ \dfrac{d}{dt}R = \tau_1 I + \tau_2 A + \phi_1 Q + \phi_2 H - \mu R, \\ \dfrac{d}{dt}M = q_1 I + q_2 A - q_3 M. \end{cases} \tag{27}$$

The limit of (27) is given by

$$\begin{cases} \dfrac{d}{dt}A = \theta\rho E^* - (\tau_2 + \mu)A^*, \\ \dfrac{d}{dt}Q = \delta_1 E^* - (\phi_1 + \delta_2 + \mu)Q^*, \\ \dfrac{d}{dt}H = \gamma I^* + \delta_2 Q^* - (\phi_2 + \xi_2 + \mu)H^*, \\ \dfrac{d}{dt}R = \tau_1 I^* + \tau_2 A^* + \phi_1 Q^* + \phi_2 H^* - \mu R^*, \\ \dfrac{d}{dt}M = q_1 I^* + q_2 A^* - q_3 M^*. \end{cases} \tag{28}$$

When system (28) is solved with the initial conditions of $A(0), Q(0), H(0), R(0), M(0)$, then as $t \longrightarrow \infty$, $A \longrightarrow A^*$, $Q \longrightarrow Q^*$, $H \longrightarrow H^*$, $R \longrightarrow R^*$, and $M \longrightarrow M^*$ which is the GAS of the endemic equilibrium. □

3.2. Bifurcation Analysis. It has been observed from stability analysis of various epidemic models that the $\mathcal{R}_0 < 1$ is the sufficient condition for wiping out infections in a

population. This condition usually holds when the system exhibits forward bifurcation. However, in considering a control intervention measure such as vaccination of the susceptibles, it has been observed that the condition $\mathscr{R}_0 < 1$ may not be sufficient to control the disease. Thus, the model transmissibility asymptomatic pattern is now determined by a quantity $\mathscr{R}_0$ defined as the effective reproduction number. It has been observed in some studies [49–53] that, there can be coexistence of the endemic and disease-free equilibrium, which are both stable for $\mathscr{R}_0 < 1$, which represents backwards bifurcation. In controlling diseases in the presence of backward bifurcation, the $\mathscr{R}_0$ has to be lowered to a value less than one. This section employs the theorem propounded by Castillo-Chavez et al. [54] to explore the type of bifurcation exhibited by the model system (1). To determine whether the phenomenon of bifurcation exists in model system (1), the centre manifold theory [54] is employed. The following necessary substitutions are taken to conform to the theorem's requirement for easier computation of the bifurcation coefficients.

We denote $x_1 = S$, $x_2 = E$, $x_3 = I$, $x_4 = A$, $x_5 = Q$, $x_6 = H$, $x_7 = R$, and $x_8 = M$ such that the total population here is given by $N = x_1 + x_2 + x_3 + x_4 + x_5 + x_6 + x_7 + x_8$. With vector notation of $X = (x_1, x_2, \cdots, x_8)^T$, the model system (1) can be redesigned in the form $dX/dt = F(X)$, with $F = (f_1, f_2, \cdots, f_8)^T$ given by

$$\begin{cases} \frac{d}{dt}x_1 = \Lambda - \mu x_1 - \eta_2 x_8 x_1 - \eta_1 \frac{x_3 x_1}{N} - \frac{\psi x_4 x_1}{N}\eta_1, \\ \frac{d}{dt}x_2 = \eta_2 x_8 x_1 + \eta_1 \frac{x_3 x_1}{N} + \frac{\psi x_4 x_1}{N}\eta_1 - ((1-\theta)\omega + \theta\rho + \delta_1 + \mu)x_2, \\ \frac{d}{dt}x_3 = (1-\theta)\omega x_2 - (\tau_1 + \xi_1 + \gamma + \mu)x_3, \\ \frac{d}{dt}x_4 = \theta\rho x_2 - (\tau_2 + \mu)x_4, \\ \frac{d}{dt}x_5 = \delta_1 x_2 - (\phi_1 + \delta_2 + \mu)x_5, \\ \frac{d}{dt}x_6 = \gamma x_3 + \delta_2 x_5 - (\phi_2 + \xi_2 + \mu)x_6, \\ \frac{d}{dt}x_7 = \tau_1 x_3 + \tau_2 x_4 + \phi_1 x_5 + \phi_2 x_6 - \mu x_7, \\ \frac{d}{dt}x_8 = q_1 x_3 + q_2 x_4 - q_3 x_8. \end{cases} \tag{29}$$

The Jacobian of the new system (29) evaluated at the DFE, denoted by $J(D_{E_0})$ is given by,

$$J(D_{E_0}) = \begin{pmatrix} -\mu & 0 & -\eta_1 & -\psi\eta_1^* & 0 & 0 & 0 & \frac{-\eta_2\Lambda}{\mu} \\ 0 & -h_{11} & \eta_1 & \psi\eta_1^* & 0 & 0 & 0 & \frac{\eta_2\Lambda}{\mu} \\ 0 & (1-\theta)\omega & -h_{22} & 0 & 0 & 0 & 0 & 0 \\ 0 & \theta\rho & 0 & -(\tau_2+\mu) & 0 & 0 & 0 & 0 \\ 0 & \delta_1 & 0 & 0 & -h_{33} & 0 & 0 & 0 \\ 0 & 0 & \gamma & 0 & \delta_2 & -h_{44} & 0 & 0 \\ 0 & 0 & \tau_1 & \tau_2 & \phi_1 & \phi_2 & -\mu & 0 \\ 0 & 0 & q_1 & q_2 & 0 & 0 & 0 & -q_3 \end{pmatrix}, \tag{30}$$

where $h_{11} = ((1-\theta)\omega + \theta\rho + \delta_1 + \mu)$, $h_{22} = (\tau_1 + \xi_1 + \gamma + \mu)$, $h_{33} = (\phi_1 + \delta_2 + \mu)$, $h_{44} = (\phi_2 + \xi_2 + \mu)$. Given that $\eta_1 = \eta_1^*$ is considered as the bifurcation parameter in the case when $\mathscr{R}_0 = 1$, then expressing η_1 in terms of the other parameters when $\mathscr{R}_0 = 1$ becomes,

$$\eta_1 = \eta_1^* = \frac{\mu q_3 R_1 R_2 R_3 - (\eta_2\Lambda(1-\theta)\omega q_1 q_3 + \theta\rho\eta_2\Lambda q_2 R_2)}{\mu q_3(\psi\theta\rho R_2 + (1-\theta)\omega R_3)}. \tag{31}$$

Hence $J(D_{E_0})|_{\eta_1=\eta_1^*}$ has a right eigenvector denoted by $\mathscr{W} = (w_1, w_2, \cdots, w_8)^T$, with

$$\begin{aligned} w_1 &= -\frac{(\eta_1(1-\theta)\omega\mu q_3(\tau_2+\mu) + \psi\eta_1\theta\rho\mu q_3(\tau_1+\xi_1+\gamma+\mu) + b_1)}{\mu^2 q_3(\tau_1+\xi_1+\gamma+\mu)(\tau_2+\mu)}w_2, \\ w_3 &= \frac{(1-\theta)\omega}{(\tau_1+\xi_1+\gamma+\mu)}w_2, w_2 > 0, w_4 = \frac{\theta\rho}{(\tau_2+\mu)}w_2, w_5 = \frac{\delta_1}{(\phi_1+\delta_2+\mu)}w_2, \\ w_6 &= \frac{(\gamma(1-\theta)\omega(\phi_1+\delta_2+\mu) + \delta_1\delta_2(\tau_1+\xi_1+\gamma+\mu))}{(\tau_1+\xi_1+\gamma+\mu)(\phi_1+\delta_2+\mu)(\phi_2+\xi_2+\mu)}w_2, \\ w_7 &= \frac{(\tau_1(1-\theta)\omega(\phi_1+\delta_2+\mu)(\phi_2+\xi_2+\mu)(\tau_2+\mu) + b_2 + b_3 + b_4)}{\mu(\tau_1+\xi_1+\gamma+\mu)(\phi_1+\delta_2+\mu)(\phi_2+\xi_2+\mu)(\tau_2+\mu)}w_2, \\ w_8 &= \frac{(1-\theta)\omega(\tau_2+\mu) + q_2\theta\rho(\tau_1+\xi_1+\gamma+\mu)}{q_1(\tau_1+\xi_1+\gamma+\mu)(\tau_2+\mu)}w_2, \end{aligned} \tag{32}$$

where

$$\begin{aligned} b_1 &= \eta_2\Lambda((1-\theta)\omega(\tau_2+\mu) + q_2\theta\rho(\tau_1+\xi_1+\gamma+\mu)), \\ b_2 &= \tau_2\theta\rho(\tau_1+\xi_1+\gamma+\mu)(\phi_1+\delta_2+\mu)(\phi_2+\xi_2+\mu), \\ b_3 &= \phi_1\delta_1(\tau_1+\xi_1+\gamma+\mu)(\phi_2+\xi_2+\mu)(\tau_2+\mu), \\ b_4 &= \gamma(1-\theta)\omega(\phi_1+\delta_2+\mu) + \delta_1\delta_2(\tau_1+\xi_1+\gamma+\mu). \end{aligned} \tag{33}$$

Further, $J(D_{E_0})|_{\eta_1=\eta_1^*}$ has a left eigenvector $\mathscr{V} = (v_1, v_2, \cdots, v_8)^T$, where $v_1 = v_5 = v_6 = v_7 = 0$, $v_2 > 0$, $v_3 = ((\eta_1 q_3\mu + q_1\eta_2\Lambda)/q_3(\tau_1+\xi_1+\gamma+\mu)\mu)v_2$, $v_4 = ((\psi\eta_1 q_3\mu + q_2\eta_2\Lambda)/q_3(\tau_2+\mu)\mu)v_2$, $v_8 = (\eta_2\Lambda/q_3\mu)v_2$.

The newly translated model Equation (29) with the bifurcation parameter $\eta_1 = \eta_1^*$ has at least one eigenvalue zero, and it affirms the existence of bifurcation in the transformed model (29). As expounded by Castillo-Chavez and Song ([54], refer to Theorem 5.1.), the equations

$$\begin{aligned} \mathbf{a} &= \sum_{k,i,j=1}^{n} v_k w_i w_j \frac{\partial^2 f_k}{\partial x_i \partial x_j}(\eta_1^*, \mathbf{0}), \\ \mathbf{b} &= \sum_{k,i,j=1}^{n} v_k w_i \frac{\partial^2 f_k}{\partial x_i \partial \eta_1}(\eta_1^*, \mathbf{0}), \end{aligned} \tag{34}$$

are the principal determinants of the direction of bifurcation (whether backwards or forward bifurcation) in the transformed system (29). When $\mathbf{a} > 0$ and $\mathbf{b} > 0$, then the bifurcation is backward and when $\mathbf{a} < 0$ and $\mathbf{b} > 0$, the bifurcation is forward.

The bifurcation coefficients are obtained as

$$\mathbf{a} = \nu_2 w_1 w_2 \left(\frac{(1-\theta)\omega(\tau_2+\mu)q_3\eta_1 + \theta\rho\psi(\tau_1+\xi_1+\gamma+\mu)q_3\eta_1 + ((1-\theta)\omega(\tau_2+\mu) + q_2\theta\rho(\tau_1+\xi_1+\gamma+\mu))\eta_2}{q_3(\tau_1+\xi_1+\gamma+\mu)(\tau_2+\mu)} \right),$$
$$\mathbf{b} = \nu_2 \Lambda w_2 \left(\frac{(1-\theta)\omega(\tau_2+\mu) + \psi\theta\rho(\tau_1+\xi_1+\gamma+\mu)}{\mu(\tau_1+\xi_1+\gamma+\mu)(\tau_2+\mu)} \right). \tag{35}$$

Assuredly, $\mathbf{a} < 0$, since $w_1 < 0$. $\mathbf{b}$ is always positive. Hence, it can be concluded that model (29) exhibits forward bifurcation as shown in Figure 1.

3.3. Local Sensitivity Analysis. Due to the fact that epidemic model's parameter values change, qualitative sensitivity analysis is necessary in order to determine the influence of parameters on model's behaviour. The analysis sensitivity reveals the criticality of each parameter of $\mathscr{R}_0$ to the model system (1). Sensitivity analysis is usually employed to bring to bear, the model's parameters with strong influence on the $\mathscr{R}_0$ that needs to be worked on in ushering in control measures. The indices from sensitivity computation assist us in quantifying the relative change in a variable with a change in the parameter. Hence, we will consider the normalized forward sensitivity index for model system (1), defined as the ratio of the relative change in the variable to the change in the parameter.

Definition 3. For a given parameter σ, the normalized forward sensitivity index of $\mathscr{R}_0$ is computed using the formula discussed in [55, 56] as;

$$\varsigma_\sigma^{\mathscr{R}_0} = \frac{\partial \mathscr{R}_0}{\partial \sigma} \frac{\sigma}{\mathscr{R}_0}. \tag{36}$$

We will use Equation (36) and parameter values from Table 1 to derive the sensitivity indices of the parameters of the model system (1) as presented in Table 2.

The sensitivity indices computation from Table 1 gives fascinating values for different parameters, and we can make some inferences. Thus, parameters with positive indices have the strength to make the number of the COVID-19 cases rise since they increase the $\mathscr{R}_0$. Additionally, the negative sensitivity indices' parameters help lower the COVID-19 epidemic because they lower the $\mathscr{R}_0$. Further, parameters with +1 sensitivity indices increase or decrease $\mathscr{R}_0$ by the same percentage as the parameters' percentages. Figures 2 and 3 further presents the influence of various combinations of parameters on the basic reproduction number, $\mathscr{R}_0$.

4. Development of Optimal Control Model

To generate control strategies to wrestle the disease from existence, we employ optimal control theory. For the assessment of the conditions necessary to determine the feasible optimal control in the COVID-19 model (1), we apply Pontryagin's maximum principle [57]. We note that, personal protection, vaccination of the susceptible population, and spraying the environment with disinfectant have significantly been encouraged during the COVID era. Hence, to add control strategies to the study, we rebuild the model (1) by reducing the transmission rate by a factor $(1-u_1)$. We consider further the vaccination control denoted by u_2 for the susceptibles and a control for disinfection of the environment represented by u_3. Hence, the new formulated optimal control model of model system (1) becomes;

$$\begin{cases} \frac{d}{dt}S = \Lambda - \mu S - (1-u_1)\eta_2 MS - (1-u_1)\eta_1 \frac{\mathrm{IS}}{N} - (1-u_1)\frac{\psi AS}{N}\eta_1 - u_2 S, \\ \frac{d}{dt}E = (1-u_1)\eta_2 MS + (1-u_1)\eta_1 \frac{\mathrm{IS}}{N} + (1-u_1)\frac{\psi AS}{N}\eta_1 - ((1-\theta)\omega + \theta\rho + \delta_1 + \mu)E, \\ \frac{d}{dt}I = (1-\theta)\omega E - (\tau_1 + \xi_1 + \gamma + \mu)I, \\ \frac{d}{dt}A = \theta\rho E - (\tau_2 + \mu)A, \\ \frac{d}{dt}Q = \delta_1 E - (\phi_1 + \delta_2 + \mu)Q, \\ \frac{d}{dt}H = \gamma I + \delta_2 Q - (\phi_2 + \xi_2 + \mu)H, \\ \frac{d}{dt}R = \tau_1 I + \tau_2 A + \phi_1 Q + \phi_2 H + u_2 S - \mu R, \\ \frac{d}{dt}M = q_1 I + q_2 A - q_3 M - u_3 M, \\ \text{with } S \geq 0, E \geq 0, I \geq 0, A \geq 0, Q \geq 0, H \geq 0, R \geq 0 \text{ and } M \geq 0. \end{cases} \tag{37}$$

The controls $u(t) = u_i \in \mathscr{U}$ are bounded and Lebegue measurable.

The objective here is to minimize $\mathscr{J}$ given by

$$\mathscr{J} = \int_0^{t_f} \left[B_1 E + B_2 I + B_3 A + \frac{1}{2}h_1 u_1^2 + \frac{1}{2}h_2 u_2^2 + \frac{1}{2}h_3 u_3^2 \right] dt, \tag{38}$$

subject to model system (37). We assign factors B_1, B_2, B_3, h_1, h_2, and h_3 in the integrand of (18) as coefficients that serve as weight that balance Equation (38). The coefficients B_1, B_2, B_3, h_1, h_2, and h_3 estimate the cost of ushered in interventions that need to be taken over the time of $[0, T]$. We determine an optimal control u_1^*, u_2^*, u_3^* such that

$$\mathscr{J}(u_1^*, u_2^*, u_3^*) = \min_{\mathscr{U}} \mathscr{J}(u_1, u_2, u_3), \tag{39}$$

with $\mathscr{U}$ subject to the model system (37). We use the

Table 1: COVID-19 model parameters and description.

Parameter	Values	Source
Λ	μN(0)	Assumed
η_1	0.003	[1]
ψ	0.004	[1]
ω	0.00001111	[1]
τ_1	0.00023	[1]
q_1	0.00101	[1]
q_3	0.23008	[1]
ξ_1	0.0002	[1]
ϕ_1	0.1	[1]
δ_2	0.06	[1]
μ	0.000035	[1]
η_2	3.4002×10^{-7}	[1]
θ	0.21003	[1]
ρ	0.0180322	[1]
τ_2	0.19	[1]
q_2	0.0214	[1]
δ_1	0.1233	[1]
γ	0.0005	[1]
ϕ_2	0.2	[1]
ξ_2	0.01	[1]

most explored method in optimal control modelling, Pontryagin maximum principle [57], and find the solution and the necessary conditions of the optimal control problem (37).

4.1. Existence of the Optimal Controls. Related to the result of Fleming and Rishel as provided in [58], the existence of optimal control triple that minimizes (38) subject to (37) is shown.

Table 2: Parameters for $\mathscr{R}_0$ and their sensitivity index for model (1).

Parameter	Sensitivity index	Parameter	Sensitivity index
Λ	0.9956	ω	$8.1966 \times 1\ 0^{-5}$
η_1	0.0044	τ_2	0.9998
η_2	0.9956	τ_1	$3.2276 \times 1\ 0^{-6}$
ψ	0.0044	γ	$7.0166 \times 10 - 6$
q_1	5.5293×10^{-7}	μ	-0.9951
q_2	0.9956	$q\ 3$	0.9956
ρ	1.0295	ξ_1	$2.8067 \times 1\ 0^{-6}$
θ	1.0295	$\delta\ _1$	0.9613

Theorem 4. *There exists an optimal control $u^* = (u_1^*, u_2^*, u_3^*)$ that minimizes the objective functional (38).*

The existence of the optimal control can be proved by showing that, the following conditions hold.

(D1) The set of controls is convex and closed.

(D2) The system (37) is bounded by a linear function in both the state and control variables.

(D3) The integrand in the objective functional (38) is convex with respect to the control.

(D4) There exist constants $k_1, k_2 \geq 0$ and $k_3 \geq 1$ that make the integrand in the objective functional (38) bounded by $k_1 \left(\sum_{i=1}^{2} |u_i|^2\right)^{k_3/2} - k_2$.

Proof. We construct the proof in steps as follows:

(D1): The control set $U = [0, 1]^3$ is closed. Again, we let $v, y \in U$, so that $v = (v_1, v_2, v_3)$ and $y = (y_1, y_2, y_3)$. Then, for every $\pi \in [0, 1]$, we have $\pi v_i + (1 - \pi) y_i \in U$, confirming the convexity property of the control set.

(D2): The control system (37) and its related solution are represented by Φ and Θ such that $|\Phi(t, \Theta_1, u) - \Phi(t, \Theta_2, u)|$ becomes

$$
\begin{aligned}
&\left|-u_2(S_1 - S_2) - \mu(S_1 - S_2) - (1-u_1)\eta_2(M_1S_1 - M_2S_2) - (1-u_1)\eta_1\left(\frac{I_1S_1}{N} - \frac{I_2S_2}{N}\right) - (1-u_1)\psi\left(\frac{A_1S_1}{N} - \frac{A_2S_2}{N}\right)\eta_1\right| \\
&\quad + \left|(1-u_1)\eta_2(M_1S_1 + M_2S_2) + (1-u_1)\eta_1\left(\frac{I_1S_1}{N} - \frac{I_2S_2}{N}\right) + (1-u_1)\psi\left(\frac{A_1S_1}{N} - \frac{A_2S_2}{N}\right)\eta_1 - ((1-\theta)\omega + \theta\rho + \delta_1 + \mu)(E_1 - E_2)\right| \\
&\quad + |(1-\theta)\omega(E_1 - E_2) - (\tau_1 + \xi_1 + \gamma + \mu)(I_1 - I_2)| + |\theta\rho(E_1 - E_2) - (\tau_2 + \mu)(A_1 - A_2)| + |\delta_1(E_1 - E_2) - (\phi_1 + \delta_2 + \mu)(Q_1 - Q_2)| \\
&\quad + |\gamma(I_1 - I_2) + \delta_2(Q_1 - Q_2) - (\phi_2 + \xi_2 + \mu)(H_1 - H_2)| + |\tau_1(I_1 - I_2) + \tau_2(A_1 - A_2) + \phi_1(Q_1 - Q_2) + \phi_2(H_1 - H_2) + u_2(S_1 - S_2) \\
&\quad - \mu(R_1 - R_2)| + |q_1(I_1 - I_2) + q_2(A_1 - A_2) - q_3(M_1 - M_2) - u_3(M_1 - M_2)| \leq 2(1-u_1)\eta_2|M_1S_1 - M_2S_2| + 2(1-u_1)\eta_1 \\
&\quad \ddot{A}\left|\left(\frac{I_1S_1}{N} - \frac{I_2S_2}{N}\right)\right| + 2\psi\eta_1(1-u_1)\left|\left(\frac{A_1S_1}{N} - \frac{A_2S_2}{N}\right)\right| + \mu|S_1 - S_2| + (2(1-\theta)\omega + 2\theta\rho + 2\delta_1 + \mu)|E_1 - E_2| \\
&\quad + (2\tau_1 + 2\gamma + \xi_1 + q_1 + \mu)|I_1 - I_2| + (2\tau_2 + q_2 + \mu)|A_1 - A_2| + (2\phi_1 + 2\delta_2 + \mu)|Q_1 - Q_2| + (2\phi_2 + \xi_2 + \mu)|H_1 - H_2| + 2u_2|S_1 - S_2| \\
&\quad + \mu|R_1 - R_2| + (q_3 + u_3)|M_1 - M_2|, \leq 2(1-u_1)\eta_2|S_1(M_1 - M_2) + M_2(S_1 - S_2)| + 2(1-u_1)\eta_1|S_1(I_1 - I_2) + I_2(S_1 - S_2)| \\
&\quad + 2\psi\eta_1(1-u_1)|S_1(A_1 - A_2) + A_2(S_1 - S_2)| + (2(1-\theta)\omega + 2\theta\rho + 2\delta_1 + \mu)|E_1 - E_2| + \mu|S_1 - S_2| + (2\tau_1 + 2\gamma + \xi_1 + q_1 + \mu)|I_1 - I_2| \\
&\quad + (2\tau_2 + q_2 + \mu)|A_1 - A_2| + (2\phi_2 + \xi_2 + \mu)|H_1 - H_2| + \mu|R_1 - R_2| + (q_3 + u_3)|M_1 - M_2| + (2\phi_1 + 2\delta_2 + \mu)|Q_1 - Q_2|, \\
&\leq Y_1|S_1 - S_2| + Y_2|E_1 - E_2| + Y_3|I_1 - I_2| + Y_4|A_1 - A_2| + Y_5|Q_1 - Q_2| + Y_6|H_1 - H_2| + Y_7|R_1 - R_2| + Y_8|M_1 - M_2|,
\end{aligned}
\tag{40}
$$

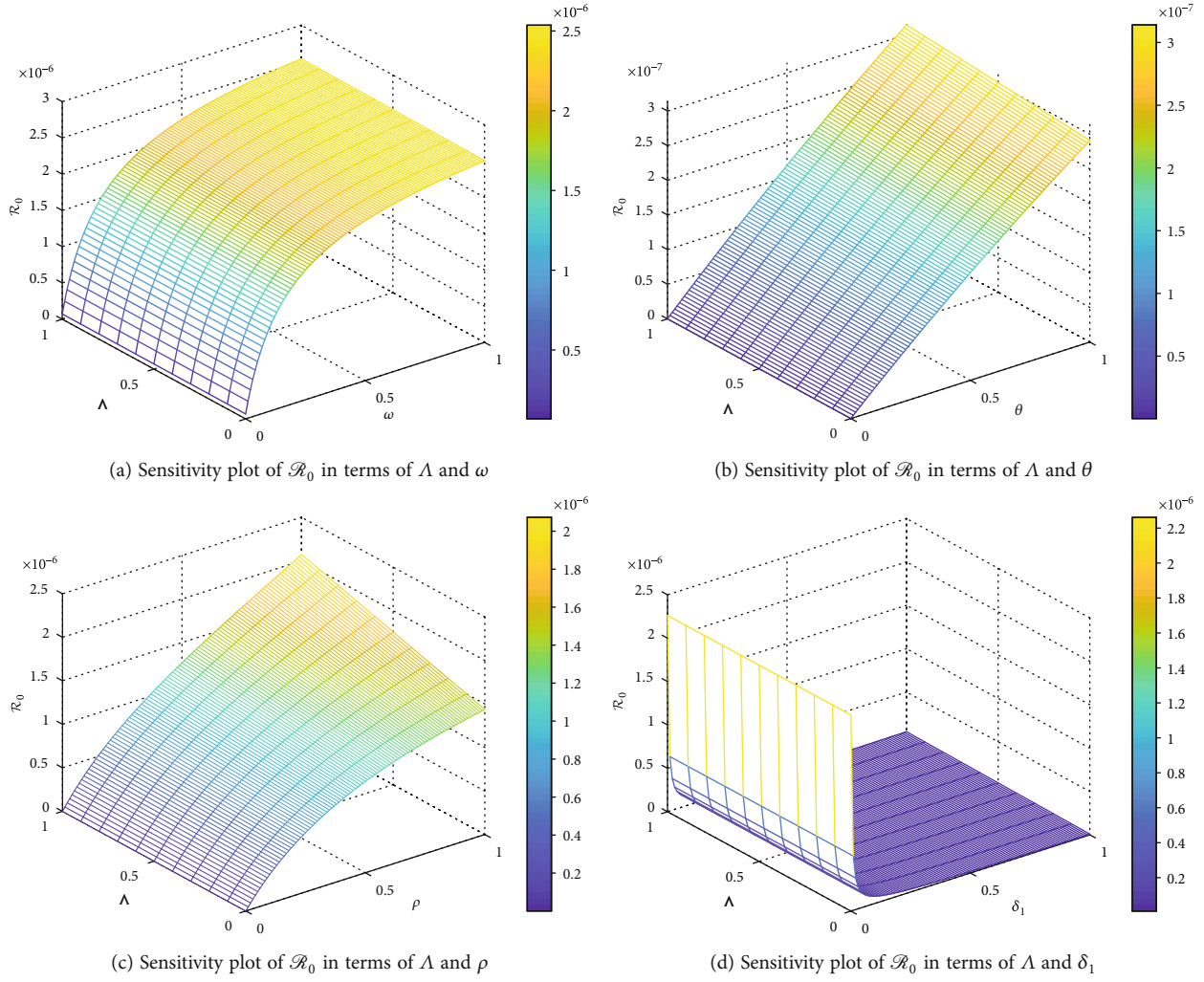

(a) Sensitivity plot of $\mathcal{R}_0$ in terms of Λ and ω

(b) Sensitivity plot of $\mathcal{R}_0$ in terms of Λ and θ

(c) Sensitivity plot of $\mathcal{R}_0$ in terms of Λ and ρ

(d) Sensitivity plot of $\mathcal{R}_0$ in terms of Λ and δ_1

FIGURE 2: Sensitivity plot of $\mathcal{R}_0$ in terms of Λ, ω, θ, ρ, and δ_1 using values in Table 2.

where $Y_1 = (2u_2 + \mu)$, $Y_2 = (2(1-\theta)\omega + 2\theta\rho + 2\delta_1 + \mu)$, $Y_3 = (2(1-u_1)(\eta_1\Lambda/\mu) + 2\tau_1 + 2\gamma + \xi_1 + q_1 + \mu)$, $Y_4 = (2\psi\eta_1(1-u_1)(\Lambda/\mu) + 2\tau_2 + q_2 + \mu)$, $Y_5 = (2\phi_1 + 2\delta_2 + \mu)$, $Y_6 = (2\phi_2 + \xi_2 + \mu)$, $Y_7 = \mu$, $Y_8 = (2(1-u_1)(\eta_2\Lambda/\mu) + q_3 + u_3)$ and $Y = \max\{Y_1, Y_2, Y_3, Y_4, Y_5, Y_6, Y_7, Y_8\}$.

Hence the Lipschitz continuous uniformity of Φ is proved.

(D3): We let the Langrangian of the objective functional (38) be $L(t, n, u)$. Then,

$$L(t, n, u) = \nu_1(t, n) + \nu_2(t, n), \tag{41}$$

with, $\nu_1(t, n) = B_1E + B_2I + B_3A$ and $\nu_2(t, n) = 1/2\sum_{j=1}^{3} h_j u_j$. The convexity of $\nu_2(t, n)$, which is a linear combination of the control function $1/2\sum_{j=1}^{3} h_j u_j$ has to be shown. We let $h(u) = 1/2u^2$ for $\lambda : [0, 1]^2 \longrightarrow R$. Then, $\forall t_1, t_2 \in [0, 1]^2$, $\rho_2 \in [0, 1]$. Hence, it follows that the below inequality holds.

$$\rho_2\lambda(t_1) + (1-\rho_2)\lambda(t_2) \geq \lambda(\rho_2 t_1 + (1-\rho_2)t_2). \tag{42}$$

This confirms the convexity of the Lagrangian with respect to the control.

(D4): By inspection, we noticed in (41) that $L(t, n, u) \geq \nu_1(t, n)$. Hence, grounded on this, we conclude that

$$L(t, n, u) \geq \frac{1}{2}h_1u_1^2 + \frac{1}{2}h_2u_2^2 + \frac{1}{2}h_3u_3^2 \geq k_1\left(\sum_{i=1}^{2}|u_i|^2\right)^{k_3/2} - k_2, \tag{43}$$

with $k_1 = 1/2\min\{h_1, h_2, h_3\}$, $k_2 > 0$ and $k_3 = 2$. This completes the proof. □

4.2. Characterization of Optimal Controls. Using the Principle translates the COVID model (37) and its associated objective functional (38) into a problem of minimizing a Hamiltonian H, with respect to the controls $u_j(t)$, for $j = 1, 2, 3$. The Hamiltonian for system (17) is given by;

$$H = L(t, n, u) + \sum_{k=1}^{8} \varsigma_k f_k. \tag{44}$$

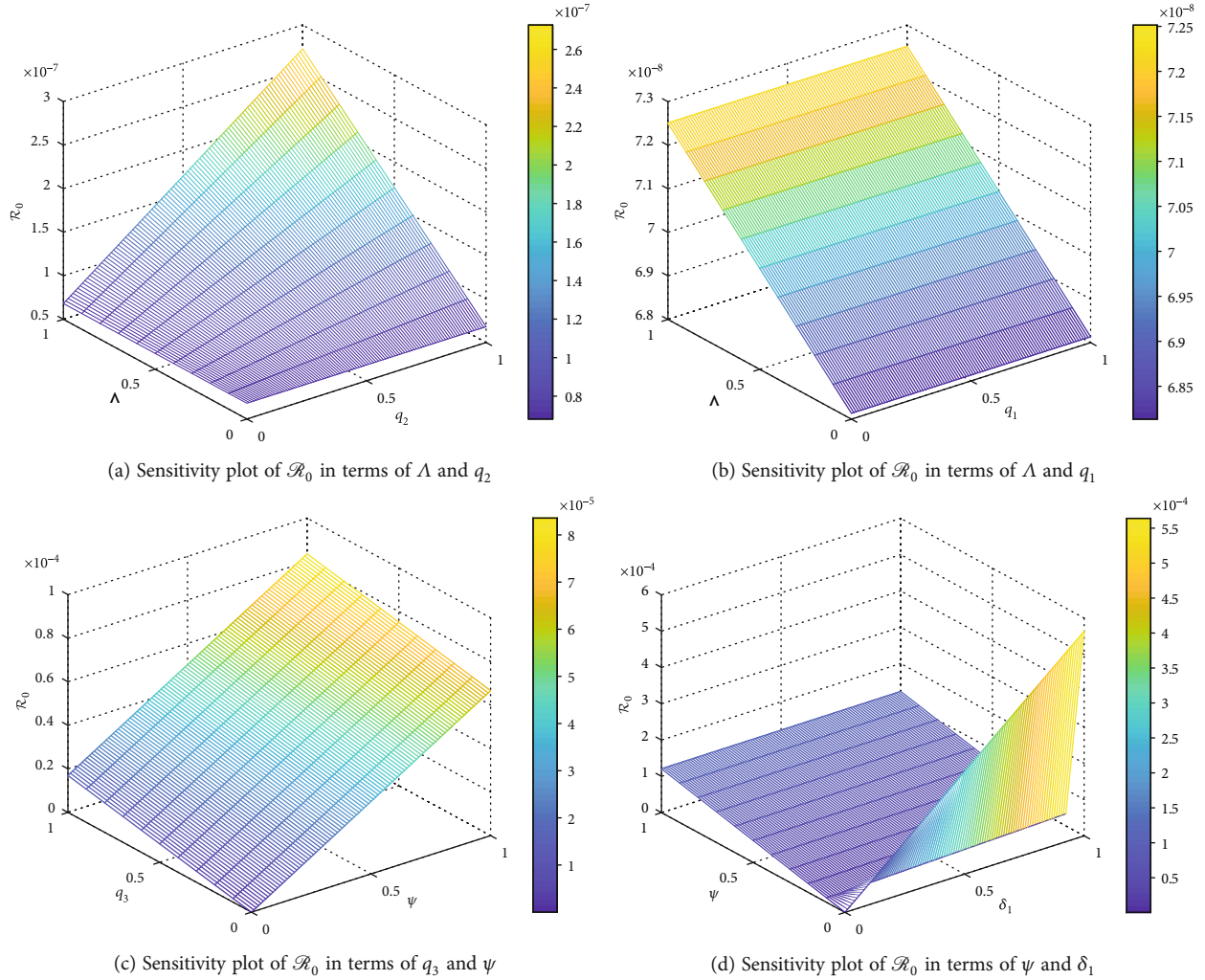

(a) Sensitivity plot of $\mathcal{R}_0$ in terms of Λ and q_2

(b) Sensitivity plot of $\mathcal{R}_0$ in terms of Λ and q_1

(c) Sensitivity plot of $\mathcal{R}_0$ in terms of q_3 and ψ

(d) Sensitivity plot of $\mathcal{R}_0$ in terms of ψ and δ_1

FIGURE 3: Sensitivity plot of $\mathcal{R}_0$ in terms of Λ, q_1, q_2, ψ and δ_1 using values in Table 2.

where the f_k in Equation (44) are the right-hand sides of system (37) and ς_k are the respective adjoint variables for the state S, E, I, A, Q, H, R, and M.

Theorem 5. *Consider the triple optimal control (u_1^*, u_2^*, u_3^*) satisfying the Condition (39), then there exist adjoint variables ς_k satisfying adjoint system below;*

$$\left.\begin{aligned}
\frac{d}{dt}\varsigma_1 &= \varsigma_1\mu + (\varsigma_1-\varsigma_2)\eta_2 M(1-u_1) + (\varsigma_1-\varsigma_2)(1-u_1)\eta_1\frac{I}{N} + (\varsigma_1-\varsigma_2)(1-u_1)\psi\frac{A}{N}\eta_1 - u_2\varsigma_7,\\
\frac{d}{dt}\varsigma_2 &= \varsigma_2\mu + (\varsigma_2-\varsigma_3)(1-\theta)\omega + (\varsigma_2-\varsigma_4)\theta\rho + (\varsigma_2-\varsigma_5)\delta_1 - B_1,\\
\frac{d}{dt}\varsigma_3 &= (\varsigma_1-\varsigma_2)(1-u_1)\eta_1\frac{S}{N} + (\varsigma_3-\varsigma_7)\tau_1 + (\varsigma_3-\varsigma_6)\gamma + (\delta_1+\mu)\varsigma_3 - q_1\varsigma_8 - B_2,\\
\frac{d}{dt}\varsigma_4 &= (\varsigma_1-\varsigma_2)(1-u_1)\psi\frac{S}{N}\eta_1 + (\varsigma_4-\varsigma_7)\tau_2 - q_2\varsigma_8 + \mu\varsigma_4 - B_3,\\
\frac{d}{dt}\varsigma_5 &= (\varsigma_5-\varsigma_7)\phi_1 + (\varsigma_5-\varsigma_6)\delta_2 + \mu\varsigma_5,\\
\frac{d}{dt}\varsigma_6 &= (\varsigma_6-\varsigma_7)\phi_2 + \xi_2\varsigma_6 + \mu\varsigma_6,\\
\frac{d}{dt}\varsigma_7 &= \mu\varsigma_7,\\
\frac{d}{dt}\varsigma_8 &= (\varsigma_1-\varsigma_2)(1-u_1)\eta_2 S + q_3\varsigma_8 - u_3\varsigma_8,
\end{aligned}\right\} \tag{45}$$

with transversality conditions

$$\varsigma_j(T) = 0, j = 1, 2, \cdots, 8. \tag{46}$$

The control functions (u_1^*, u_2^*, u_3^*) satisfies the optimality condition and is given by

$$u_i^*(t) = \min\{1, \max\{0, \Gamma_i\}\}, i = 1, 2, 3. \tag{47}$$

where

$$\begin{aligned}
\Gamma_1 &= (\varsigma_2-\varsigma_1)\frac{MS}{h_1}\eta_2 + (\varsigma_2-\varsigma_1)\frac{\mathrm{IS}}{Nh_1}\eta_1 + (\varsigma_2-\varsigma_1)\frac{AS}{Nh_1}\eta_1,\\
\Gamma_2 &= (\varsigma_1-\varsigma_7)\frac{S}{h_2},\\
\Gamma_3 &= \frac{M}{h_3}\varsigma_8.
\end{aligned} \tag{48}$$

Proof. Referring to the Hamiltonian (49), given by

$$\left.\begin{aligned} H &= \left[B_1E + B_2I + B_3A + \frac{1}{2}h_1u_1^2 + \frac{1}{2}h_2u_2^2 + \frac{1}{2}h_3u_3^2\right] \\ &+\varsigma_1\left\{\Lambda - \mu S - (1-u_1)\eta_2 MS - (1-u_1)\eta_1\frac{\mathrm{IS}}{N} - (1-u_1)\frac{\psi AS}{N}\eta_1 - u_2S\right\} \\ &+\varsigma_2\left\{(1-u_1)\eta_2 MS + (1-u_1)\eta_1\frac{\mathrm{IS}}{N} + (1-u_1)\frac{\psi AS}{N}\eta_1 - ((1-\theta)\omega + \theta\rho + \delta_1 + \mu)E\right\} \\ &+\varsigma_3\{(1-\theta)\omega E - (\tau_1 + \xi_1 + \gamma + \mu)I\} + \varsigma_4\{\theta\rho E - (\tau_2 + \mu)A\} \\ &+\varsigma_5\{\delta_1 E - (\phi_1 + \delta_2 + \mu)Q\} + \varsigma_6\{\gamma I + \delta_2 Q - (\phi_2 + \xi_2 + \mu)H\} \\ &+\varsigma_7\{\tau_1 I + \tau_2 A + \phi_1 Q + \phi_2 H + u_2 S - \mu R\} + \varsigma_8\{q_1 I + q_2 A - q_3 M - u_3 M\}, \end{aligned}\right\} \tag{49}$$

we generate the adjoint system (45) by differentiating partially the Hamiltonain (49) with respect to the corresponding state variables S, E, I, A, Q, H, R, and M as

$d\varsigma_1/dt = -\partial L/\partial S$, $d\varsigma_2/dt = -\partial L/\partial E$, $d\varsigma_3/dt = -\partial L/\partial I$, $d\varsigma_4/dt = -\partial L/\partial A$, $d\varsigma_5/dt = -\partial L/\partial Q$, $d\varsigma_6/dt = -\partial L/\partial H$, $d\varsigma_7/dt = -\partial L/\partial R$, $d\varsigma_8/dt = -\partial L/\partial M$ The characterization of the controls u_1^*, u_2^*, u_3^* as in (39) is determined by applying the equation below;

$$\frac{\partial L}{\partial u_i} = 0, i = 1, 2, 3. \tag{50}$$

Utilizing bounds on the controls by standard argument, we determine the characterization

$$u_i^* = \begin{cases} 0 & \text{if } \varphi_i^* \le 0, \\ \varphi_i^* & \text{if } 0 \le \varphi_i^* \le 1, \\ 1 & \text{if } \varphi_i^* \ge 1, \end{cases} \tag{51}$$

where

$$\begin{aligned} \varphi_1^* &= (\varsigma_2 - \varsigma_1)\frac{MS}{h_1}\eta_2 + (\varsigma_2 - \varsigma_1)\frac{\mathrm{IS}}{Nh_1}\eta_1 + (\varsigma_2 - \varsigma_1)\frac{AS}{Nh_1}\eta_1, \\ \varphi_2^* &= (\varsigma_1 - \varsigma_7)\frac{S}{h_2}, \quad \varphi_3^* = \frac{M}{h_3}\varsigma_8, \end{aligned} \tag{52}$$

This completes the proof. □

5. Numerical Experimentation and Discussion

With the aid of the forward-backwards sweep method as derived by Lenhart and Workman [59], a numerical solution to the optimality system of the control model was obtained. We offer the scenarios of different feasible control strategies to identify their effect on the dynamics of the COVID model. The backwards scheme solves the adjoint system (45) backwards in time, and the forward scheme solves (37) forward in time. In addition, the structured scheme considered the set of initial conditions related to the state variables and the boundary condition to solve the control optimality system in a simulated interval of $t \in [0,250]$. With this set in play, we consider the balancing factors of the objective functional (38) as: $B_1 = 10, B_2 = 10, B_3 = 10, h_1 = 5, h_2 = 10$, and $h_3 = 8$, and initial population $N(0) = 100000000$ for the simulation purpose. We concluded that $h_2 > h_1$ and h_3, as we assume that the cost of vaccines and implementing a vaccination program would be higher than the cost of personal protection and disinfecting the environment. Even though the model in [44] is a Fractional-order model, the authors estimated the model's parameters at $\alpha_1 = \alpha_2 = 1$. However, at $\alpha_1 = \alpha_2 = 1$, the model becomes an integer order model. Furthermore, since the study modifies model 1 to optimal control which simulated results are always compared to the noncontrol model, it becomes necessary that we consider the same parameter values as used in model 1. Hence, we would consider model [44] parameter values for the simulation.

5.1. Strategy 1 (Implementing Controls u_1,u_2, and u_3). The strategy 1 considered the controls u_1, u_2, and u_3. The simulation results are presented in Figures 4(a)–4(d) of Figure 4. We observe that, the exposed population (28) without control swiftly rose in the first five days and reached almost 8.5×10^5 within the next five days. The dynamics of the exposed graph changed after day 11. The graph began to slowly decrease until day 80 when the population seemed to have been wiped out. The exposed without control graph maintained this new level for the next 70 days and began to surge to a height of 0.6×10^5 for the next 65 days when it began to decrease for the rest of the simulated time smoothly. Also, the infected population without control (See Figure 4(b)) gradually rose in the first 10 days until day 50 when it began to decrease with an estimated infected population of 250. It decreased slowly to 240 in 170 days and picked up after the 170. The asymptomatically infected graph of (See Figure 4(c)) sharply increased in 10 days to reach a population of about 14500 and then decreased slowly after day 25 and reached the lower bound at 90 days. The level was maintained until 150 days when it smoothly increased for the remaining simulated time. The exposed population under controls (Figure 4(a)) decreased slowly and was expected to wipe out in 20 days completely. The infected population with control (See Figure 4(b)) increased in a similar pattern slowly in the first 10 days and decreased slightly, with the population recognized to be a little below 90 at the final time. The asymptomatically infected population with control (See Figure 4(c)) was the same as that without controls for the first 5 days but is reduced after 40 days. From the control profile graph (Figure 4(d)), u_1, which represents the personal protection control, starts from the upper bound but drops suddenly to the lower bound at the initial zero days until 60 when it swiftly moves to the upper bound. The next 190 days remained at the upper bound and then returned to the lower bound at the final time of 250 days. The vaccination control, u_2, remained at the lower bound until 59 days when it moved to the upper bound. It stayed at the upper bound until 200 days and then dropped to the lower bound and remained there for the rest of the time. u_3, denoting disinfectant control, started at the lower bound and picked to the upper bound after 60 days. It remained at the upper bound for the remaining time until 249 days, when it dropped to the lower bound.

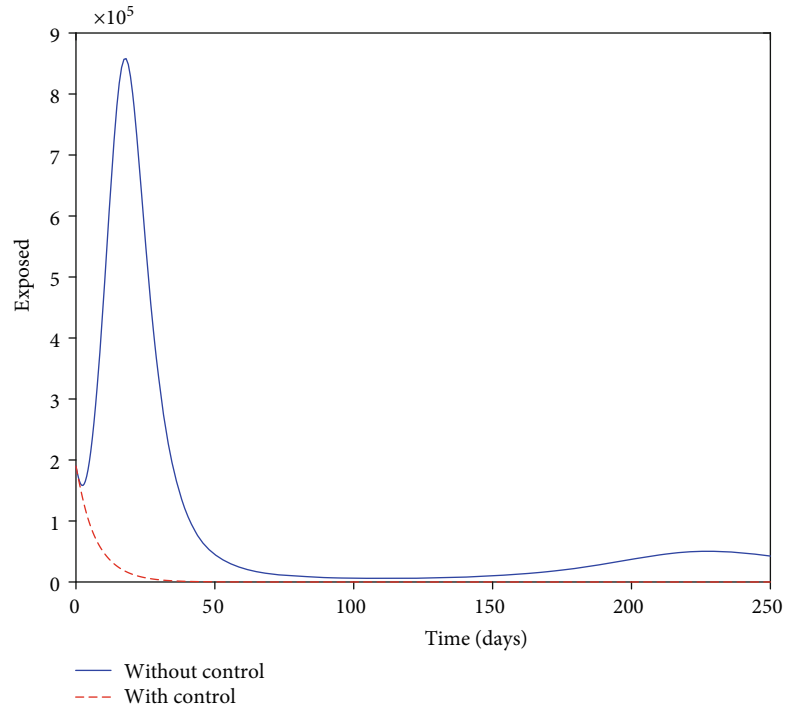

(a) The solution path of the exposed

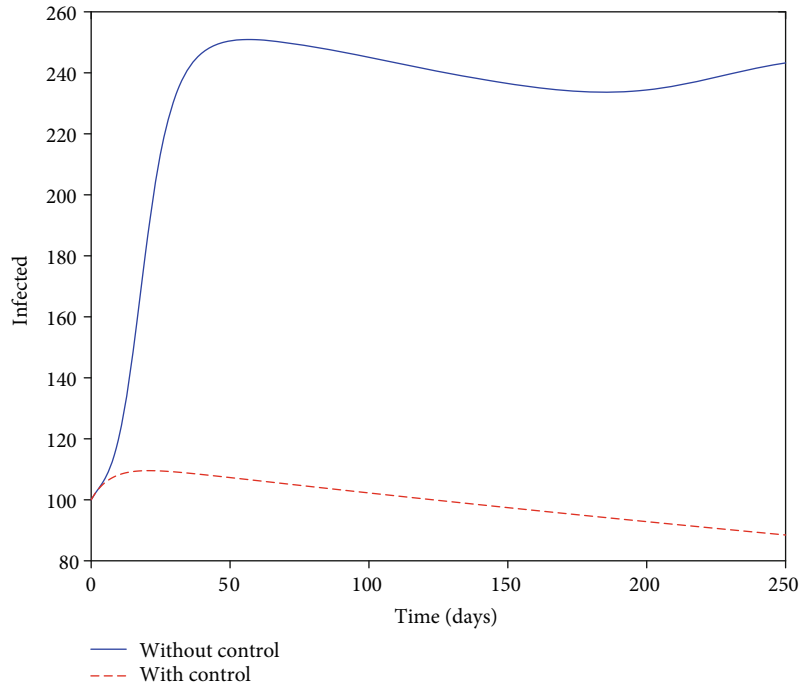

(b) The solution path of the infected

Figure 4: Continued.

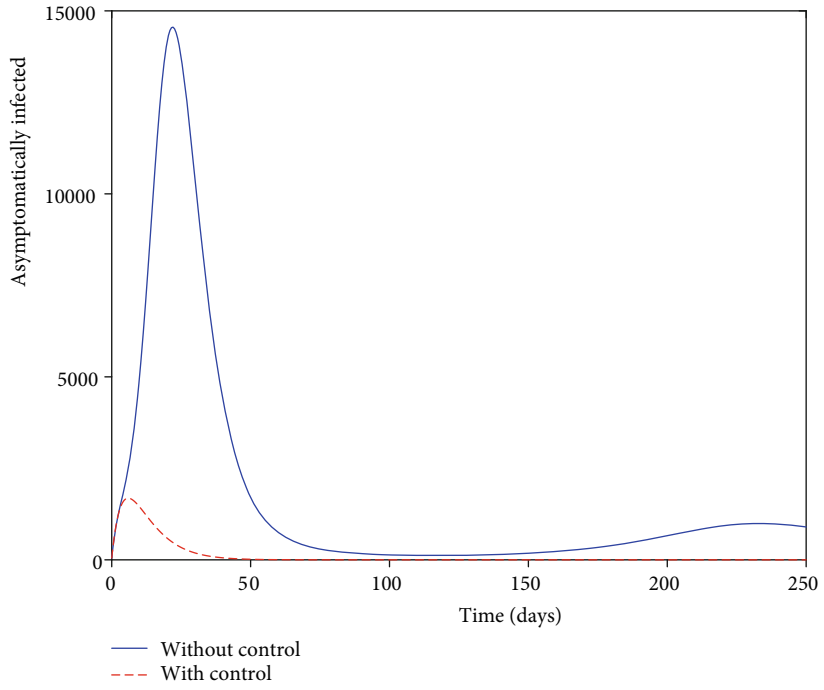

(c) The solution path of the asymptomatically infected

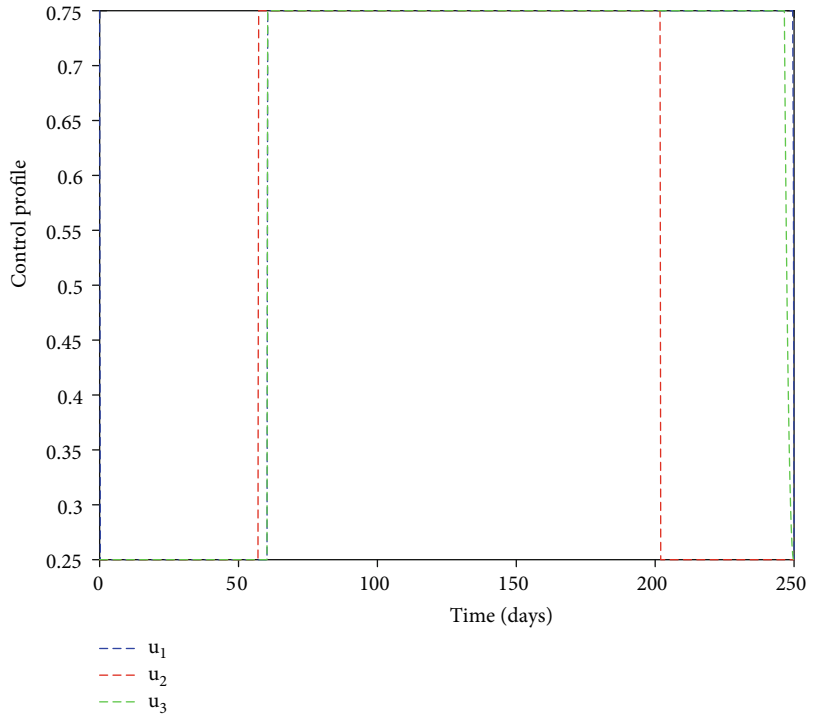

(d) Control profile

Figure 4: Graphs of simulation results for strategy 1 (with $u_1 \neq 0$, $u_2 \neq 0$, and $u_3 \neq 0$).

5.2. Strategy 2 (Implementing Controls u_1 and u_2). The strategy 2 sets u_3, the disinfectant control to zero and experiments with the controls u_1 and u_2. The simulation results are presented in Figure 5. The exposed population without control (See Figure 5(a)) shows a sudden rise in the first 10 days. The graph rises to a peak of about 8.5×10^5 and after 10 days, decreases steeply to a minimal population of about 1×10^5 within the next 90 days and maintains this new level until 150 days when it begins to increase smoothly. The infected population without control (See Figure 5(b)) gently increases for the first 25 days to reach a maximum height of 250. The new height of the infected

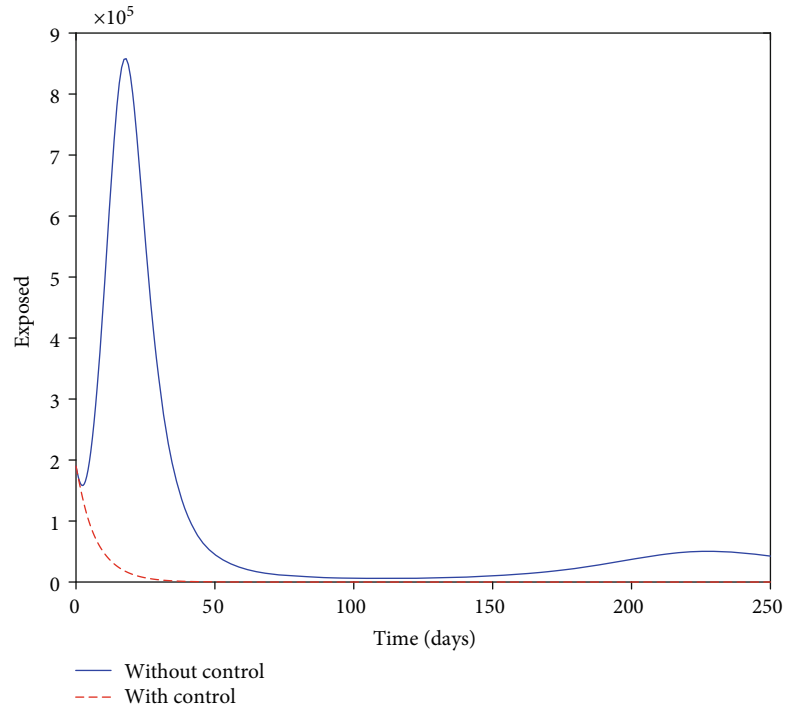

(a) The solution path of the exposed

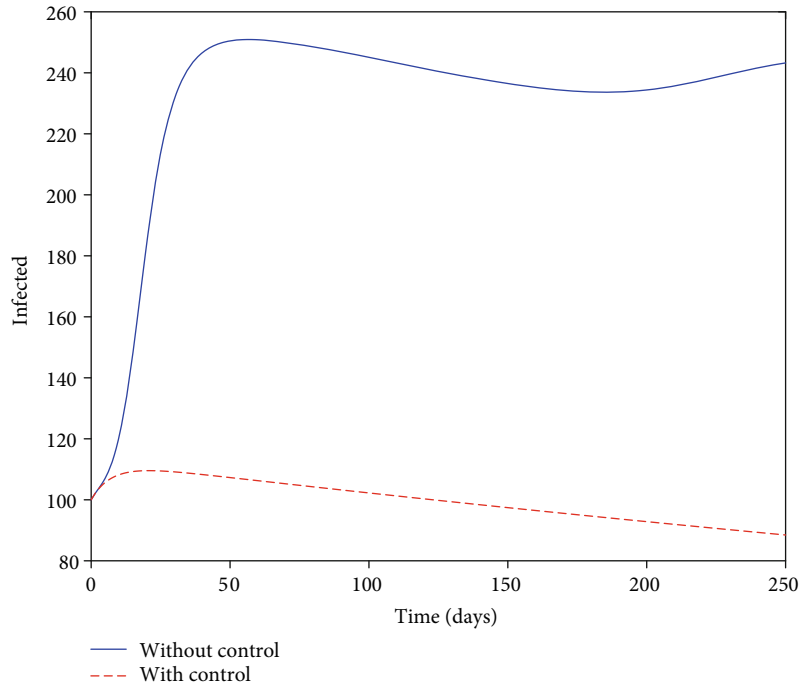

(b) The solution path of the infected

Figure 5: Continued.

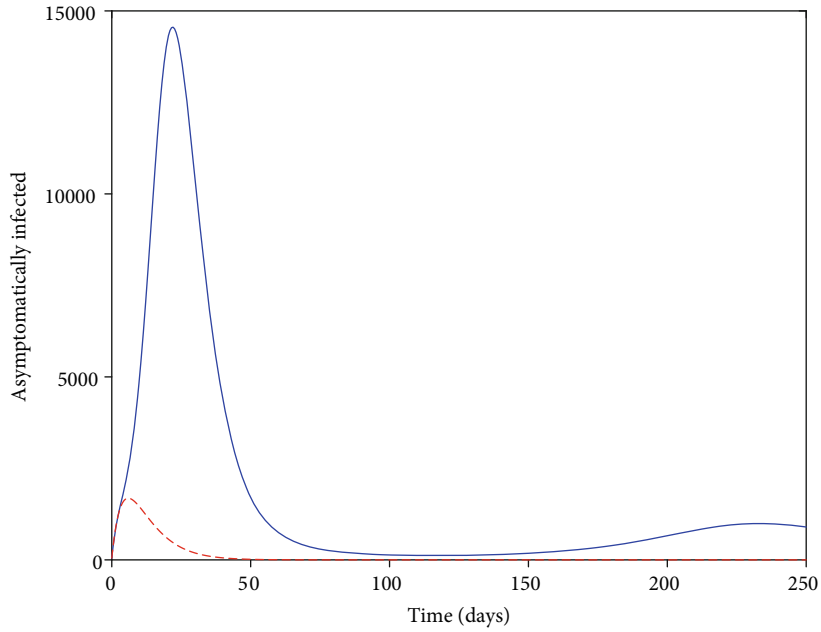

(c) The solution path of the asymptomatically infected

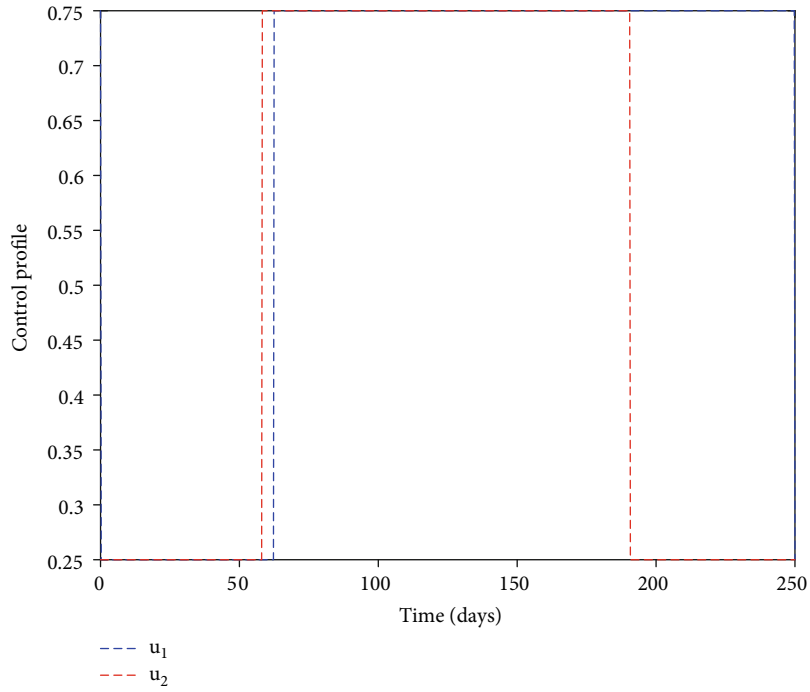

(d) Control profile

FIGURE 5: Graphs of simulation results for strategy 2 (with $u_1 \neq 0$ and $u_2 \neq 0$).

became unstable after the next 25 days, and that resulted in the population slowly decreasing to 240 in the next 150 days, after which it began to rise for the remaining time. With the asymptotically infected without control (See Figure 5(c)), we noted a quick rise of the curve in the first 10 days and reached the pinnacle at 14500 in 25 days at the infection hotspots.

The exposed population yielded to the design experiment strategy 2. The exposed population starts with 1.9×10^5 population and gently reduces until 25 days when it seems to have been wiped from the system. The infected population under control strategy 2 slightly increased in the early days and began to lower after 10 days. The graph decreased in that pattern and reached a lower height of 90 at the final time. Also,

the asymptotically infected population increased to about 2000 in the first 5 days, decreased slowly to zero in 30 days, and maintained that level for the remaining period of the simulation time. Figure 5(d) presents the control profile for Strategy 2. By inspection, we observed that the personal protection control u_1 falls to the lower bound at the initial zero time. It remained on the lower bound for 60 days when it suddenly moved to the upper bound. It then remained at the upper bound until 250 days when it dropped to the lower bound again. Control u_2, representing the vaccination control, remained at the lower bound for the first 59 days when it swiftly moved to the upper bound. It stayed at the upper bound for the next 120 days when it dropped to the lower bound and remained there for the remaining time.

5.3. Strategy 3 (Implementing Controls u_1 and u_3). With u_2 set to zero, strategy 3 uses the controls u_1 and u_3 for the experimentation by simulating the optimality system with the structured interval. The simulation results for this strategy are presented in Figure 6. We observe that, the exposed population without control (See Figure 6(a)) moved sharply to 8.5×10^5 in day 10 of the simulated time and then decreased gradually to almost 0.1×10^5 and maintained the level until 150 days when it began to rise for the remaining time. The infected population without control (See Figure 6(b)) increased slowly and moved to a height of 250 for 50 days. The population then decreased slowly for the next 100 days and began to pick up after the 100 days. The asymptomatically infected population without control (See Figure 6(c)) also shoots quickly in the first 25 days to its maximum of 14500. The dynamics changed, and the population began to reverse slowly to a level of about 100, and then picked up after 150 days and smoothly increased to the final time. The optimal control plot of the exposed produced a graph that seemed to wane in the early days but began to rise after 30 days to meet the noncontrol graph at 70 days. The level of the controlled exposed population was maintained until the final time. The infected population with control Strategy 3 (See Figure 6(b)) got lowered in the early days and continued till the final time of the simulation. The controlled population of asymptotically infected persons (See Figure 6(c)) got depleted in the first 30 days. However, for the uncontrolled problem, the population resurged and maintained the level for the rest of the simulation time. From Figure 6(d), u_1 denoting personal protection control drops suddenly from the upper bound to the lower bound at time $t = 0$. It then remained at the lower bound for 15 days and shot to the upper bound, where it remained for 15 days and dropped to the lower bound. It remained in the lower bound for another 15 days and moved to the upper bound. It then stayed at the upper bound for 15 days and dropped to the lower bound. It picked after 5 days to the upper bound and stayed there until it dropped to the lower bound. u_3 denoting disinfectant control started from the lower bound and moved to the upper bound after 15 days. It dropped to the lower bound after 15 days and again moved to the upper bound after 15. It stayed at the upper bound for another 15 days and then dropped to the lower bound for 5 days. It picked to the upper bound of 70 days and remained until the final time before dropping.

5.4. Strategy 4 (Implementing Controls u_2 and u_3). The strategy 4 set $u_1 = 0$ and utilized the control u_2 and u_3 in the numerical simulation for assigned interval. The simulation results are presented in Figures 7(a)–7(d). The Strategy 4 is observed to also do well in reducing the exposed, infected and asymptomatically infected populations. From the control profile (Figure 7(d)), the vaccination control, u_2, shot to the upper bound at time $t = 50$, stayed at the upper bound for 150 days, and then dropped to the lower bound. It remained at the lower bound for the rest of the simulated time. The disinfectant spraying control u_3 stayed at the lower bound from day 0 to 50, rocketed to the upper bound and remained there until 249 days when it returned to the lower bound.

6. Economic Cost Analysis of the Control Implementation

With the simulation results of the optimality control problem, the present section seeks to identify the strategy among the considered strategies that minimize the cost involved in executing the strategy yet give a satisfying performance output. To identify the most cost-effective strategy, we compare strategies 1, 2, 3, and 4. The approach outlined in related previous studies [60–63] is adopted to examine the average cost-effectiveness ratio (ACER) and incremental cost-effectiveness ratio (ICER) of strategies 1, 2, 3, and 4. The ICER is the ratio of the differences in cost of two control strategies to the differences in infection averted by executing that strategy. On the other hand, the ACER is the ratio of the total cost involved in executing the strategy to the total infected prevented. The mathematical formulation

$$\text{ICER} = \frac{\text{Difference in costs of control strategies } e_1 \text{ and } e_2}{\text{Difference in infection averted by the strategies}}, \tag{53}$$

is used to exhibit the number of infections averted, and the related cost of executing the strategies under consideration in increasing order of magnitude of the infection averted is presented in Table 3.

The ICER representations are derived as follows;

$$\begin{aligned}
\text{ICER}(1) &= \frac{6.1523 \times 10^3}{5.0326 \times 10^7} = 1.2225 \times 10^{-4},\\
\text{ICER}(2) &= \frac{(3.8281 - 6.1523) \times 10^3}{(5.0826 - 5.0326) \times 10^7} = -4.6484 \times 10^{-3},\\
\text{ICER}(4) &= \frac{(4.0048 - 3.8281) \times 10^3}{(5.0960 - 5.0826) \times 10^7} = 1.3186 \times 10^{-3},\\
\text{ICER}(3) &= \frac{(4.9606 - 4.0048) \times 10^3}{(5.69566 - 5.09600) \times 10^7} = 1.5936 \times 10^{-4}.
\end{aligned} \tag{54}$$

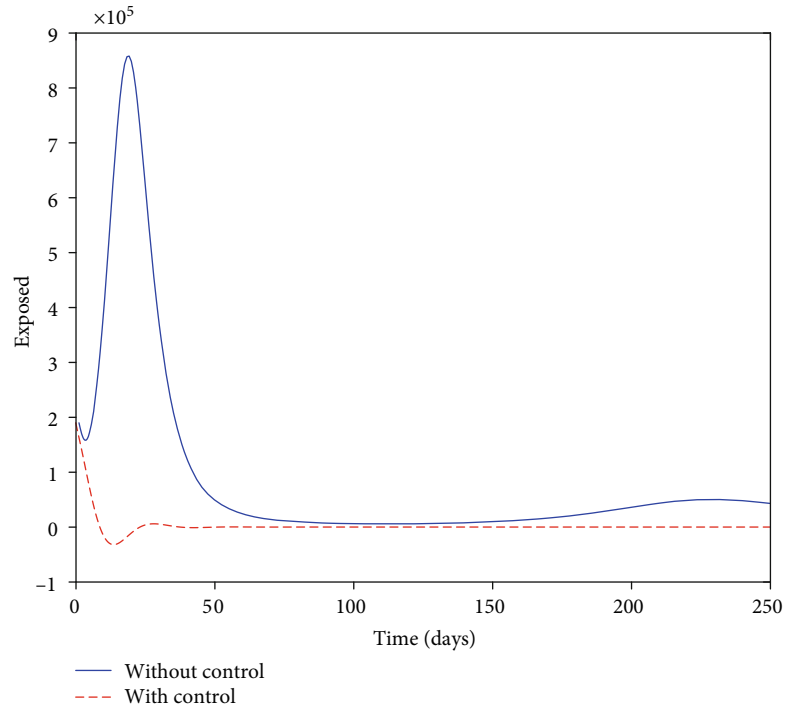

(a) The solution path of the exposed

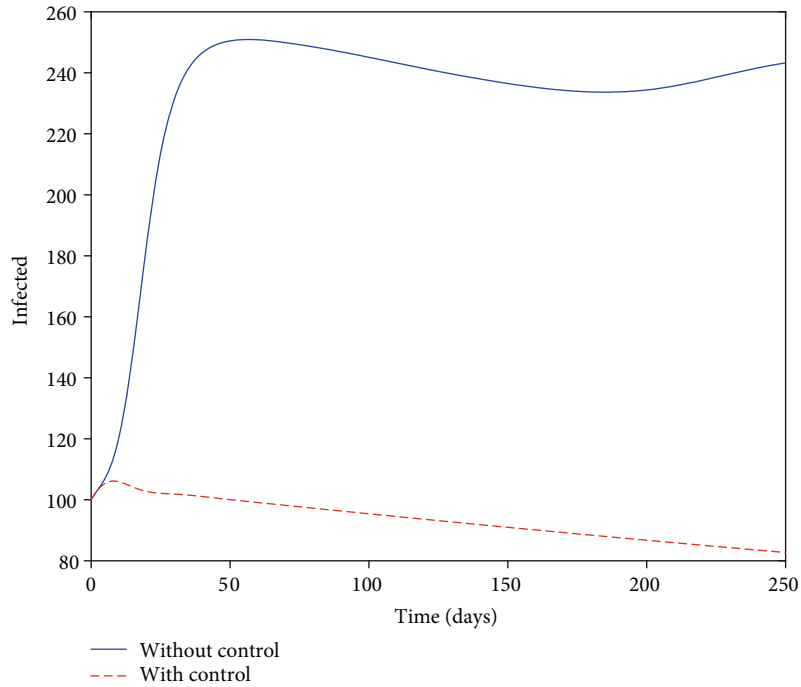

(b) The solution path of the infected

Figure 6: Continued.

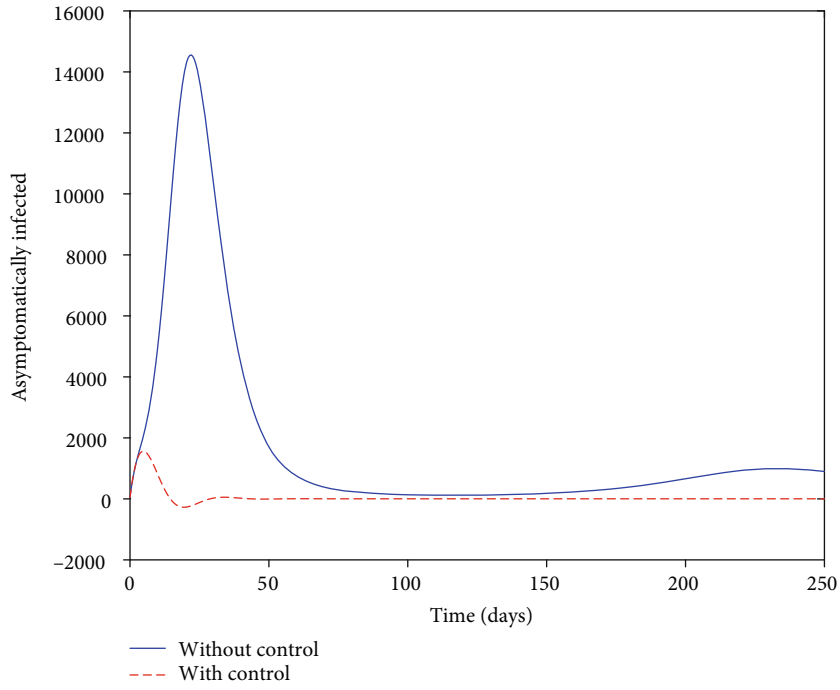

(c) The solution path of the asymptomatically infected

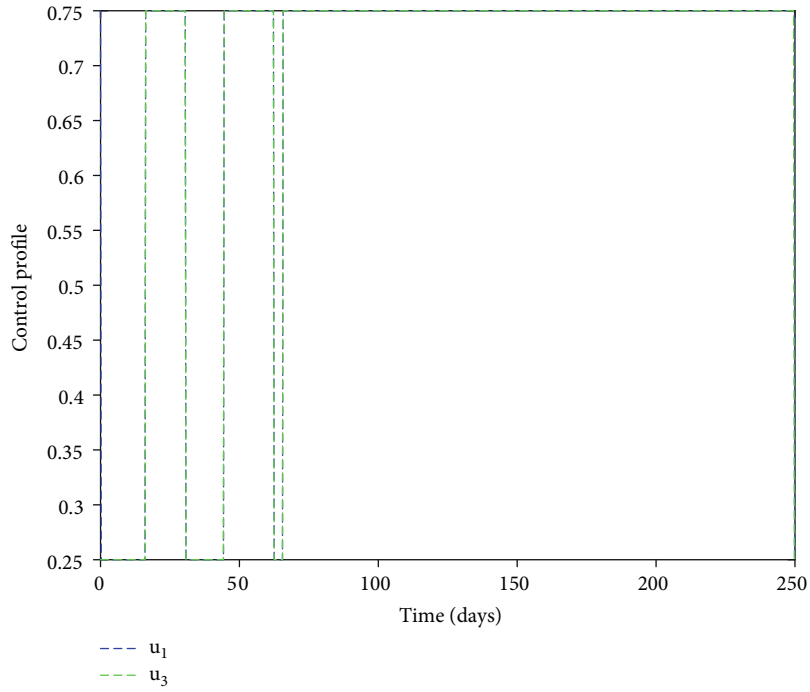

(d) Control profile

FIGURE 6: Graphs of simulation results for strategy 3 (with $u_1 \neq 0$ and $u_3 \neq 0$).

From Table 3, we notice that the ACER value of strategy 2 is the least among the strategies considered. The ACER values insinuate that strategy 2 is the most cost-effective. Further, we observe that strategy 1 has the highest ACER value, which is the least cost-effective measure. However, an in-depth analysis of the least cost-effective measure was required. The ICER of the strategies was then computed. The ICER computations depicted that strategy 1 is more costly but less effective than strategy 2. The analysis confirmed that ICER of strategy 1 is higher than ICER of strategy 2. Hence, the control strategy 1 is deleted from the considered strategies, and the remaining strategies ICERs are recalculated for further analysis on the three. The analysis of the remaining strategies is presented in Table 4.

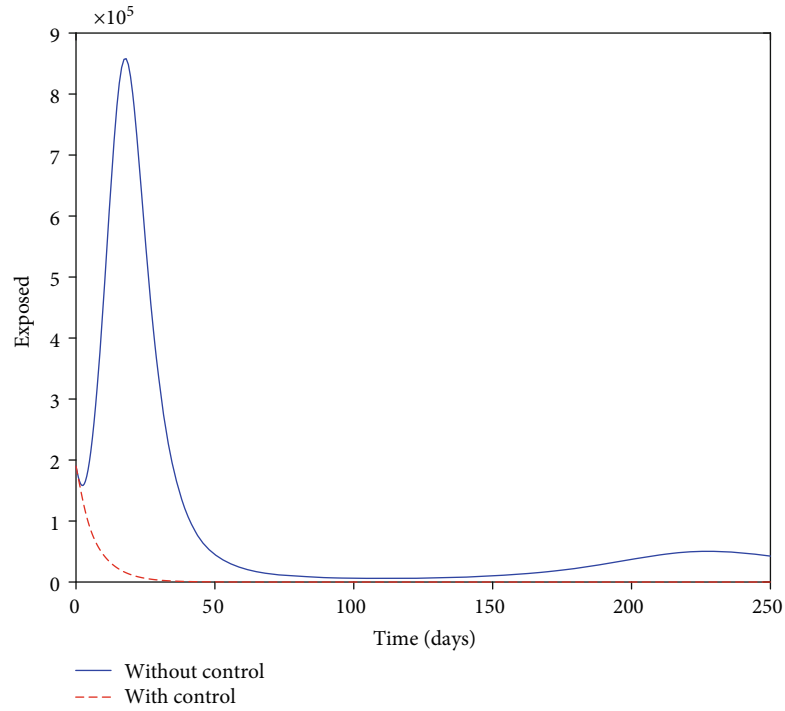

(a) The solution path of the exposed

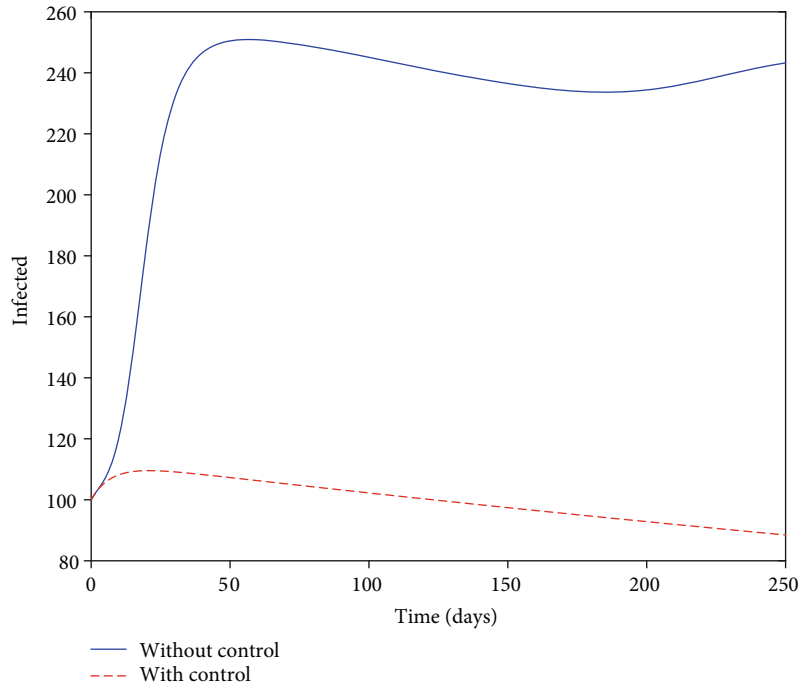

(b) The solution path of the infected

Figure 7: Continued.

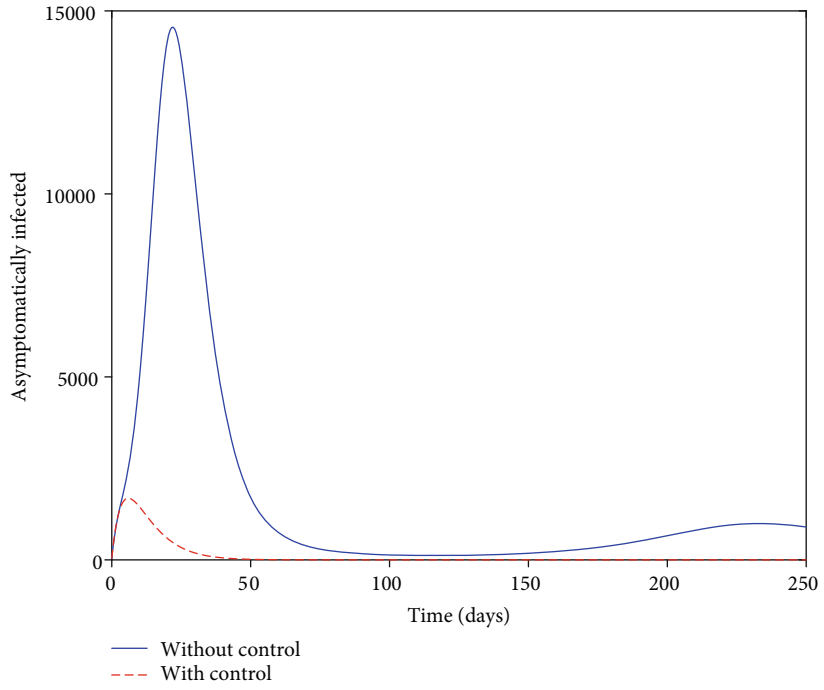

(c) The solution path of the asymptomatically infected

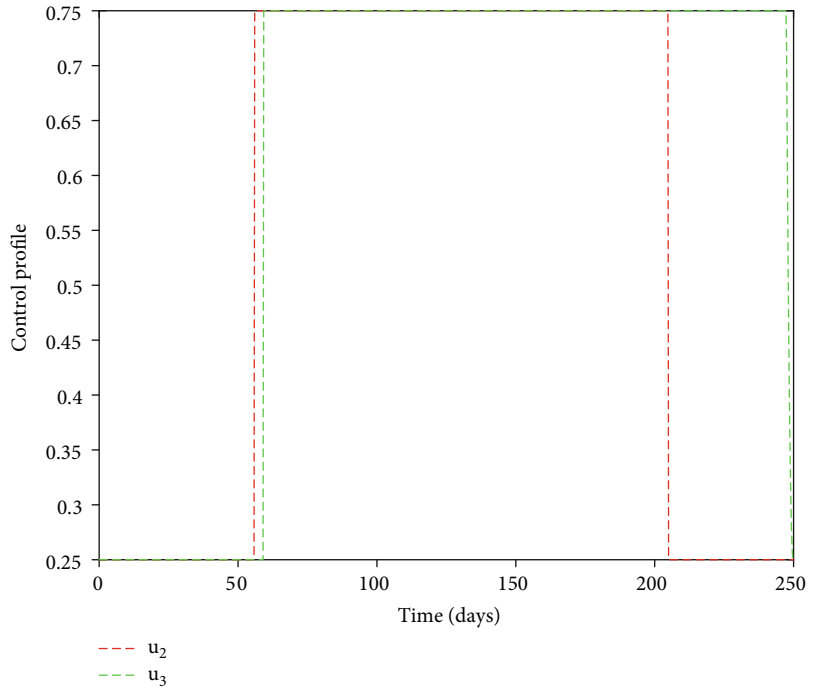

(d) Control profile

FIGURE 7: Graphs of simulation results for strategy 4 (with $u_2 \neq 0$ and $u_3 \neq 0$).

From the computed ICERs of Table 5, we see that strategy 4 ICER is higher than strategy 2. The cross-examination of the two ICER shows the dominance of strategy 2 over strategy 4. Thus, strategy 2 costs less and performs best in managing the disease. Hence, strategy 4 is removed from the remaining strategies, and the ICER of strategy 2 and 3 are recalculated and analyzed, as depicted in Table 5.

The ICER computation from Table 5 indicated that strategy 3 is higher than strategy 2. The analysis further proves that strategy 2 is the most cost-effective control strategy among the listed strategies.

6.1. Conclusion. The research considered a dynamical study on a nonlinear autonomous COVID-19 model to unveil

Table 3: Total number of infections averted from the least to the highest.

Strategies	Total infection averted ($\times 10^7$)	Total cost ($\times 10^3$)	ACER	ICER
Strategy 1	5.0326	6.1523	1.2225×10^{-4}	1.2225×10^{-4}
Strategy 2	5.0826	3.8281	0.7532×10^{-4}	$-4.6484 \times 1\ 0^{-3}$
Strategy 4	5.0960	4.0048	$0.7859 \times 10\ -4$	$1.3186 \times 1\ 0^{-3}$
Strategy 3	5.6957	4.9606	$0.8709 \times 1\ 0^{-4}$	1.5936×10^{-4}

Table 4: ICER computation of strategy 2, 4, and 3.

Strategies	Total infection averted ($\times 10^7$)	Total cost ($\times 10^3$)	ICER
Strategy 2	5.0826	3.8281	0.7532×10^{-4}
Strategy 4	5.0960	4.0048	$1.3187 \times 1\ 0^{-3}$
Strategy 3	5.6957	4.9606	$1.5938 \times 1\ 0^{-4}$

Table 5: ICER computation of strategy 2 and 3.

Strategies	Total infection averted ($\times 10^7$)	Total cost ($\times 10^3$)	ICER
Strategy 2	5.0826	3.8281	0.7532×10^{-4}
Strategy 3	5.6957	4.9606	1.8472×10^{-4}

strategies that could assist in stemming the spreading of the disease. With the introduction of the control strategies: personal protection, vaccination, and disinfecting of the environment into the state model (1), the basic model was redesigned into an optimal control problem. We utilized Pontryagin's maximum principle's [57] analytic method to characterize possible controls that may help stem the epidemic from spreading. We supported the qualitative analyses with a numerical solution that employed the fourth-order Runge-Kutta method to generate numerical solutions of the control problem. The results from the executed strategies unveiled a satisfying impact on the dynamics of the exposed, asymptomatically infected, and infected individual. The strategy 1 considered the three controls of personal protection, vaccination, and disinfectant of the environment. Interestingly, the generated graphs showed the retrospective impact of the strategy on the disease's dynamics. Thus, we see substantially minimized exposed, infected, and asymptomatically infected individuals. Strategy 2 employed personal protection and vaccination control as its intervention strategy. A similar result to using strategy 1 was obtained. Regarding strategy 3, personal protection and disinfectant controls were used. The simulation produced a pleasing effect on the dynamics of the infected. Thus, the graph depicts a convincing minimized exposed, infected, and asymptomatically infected with the strategy. The strategy of 4 chose the vaccination and disinfectant of the environment. The result minimized the exposed, infected, and asymptomatically infected. A careful examination of the strategies that employed vaccination as part of the controls substantially minimized the exposed, infected, and asymptomatically infected graphs. For instance, strategy 3, which did not consider vaccination control experienced an early rise in the asymptomatically infected graph but was minimized in the long run. The results suggest that vaccines are essential pharmaceutical control strategies needed to mitigate the disease but cannot be wholly relied on due to the resistance imposed by the mutation of the virus and the vaccines efficacies waning after a short while. This is a result of the leakiness of vaccines and limited vaccination capacity. The finding is consistent with the findings of the work [43, 64, 65], which recommended that policymakers should be pragmatic in relaxing other COVID-19 mitigating protocols since the vaccine efficacies are not 100%, as evidence of reinfection after vaccination has been proved in several studies [66–68]. Finally, we assessed the various strategies' economic costs with the cost-effectiveness analysis method. The method examined the effectiveness and cost of the listed strategies considered. The analysis unveiled that the strategy 2: personal protection and vaccination control strategy is the most cost-effective method among the considered strategies. From our investigations, we recommend that a deliberate attempt should be made by public health and all stakeholders to strengthen the personal protection protocols as recommended by WHO and encourage and educate society about the benefits of being vaccinated, as vaccines reduce hospitalization [66].

Data Availability

The authors confirm that the data supporting the findings of this study are available within the article.

Conflicts of Interest

The authors declare no conflict of interest.

Acknowledgments

(i) The results in this paper form part of the PhD thesis of the first author in the Department of Mathematics of the C. K. Tedam University of Technology and Applied Sciences, Ghana. The second author is the lead supervisor. (ii) The author acknowledges the paper as part of a PhD thesis at C. K. Tedam University of Technology and Applied Sciences, titled "Mathematical modelling of COVID-19 and Vector-borne diseases with optimal control".

References

[1] K. Kim, S. Kim, and C.-Y. Park, *Food Security in Asia and the Pacific amid the COVID-19 Pandemic, ADB BRIEFS No. 139*, 2020.

[2] J. T. Wu, K. Leung, M. Bushman et al., "Estimating clinical severity of COVID-19 from the transmission dynamics in Wuhan, China," *Nature Medicine*, vol. 26, no. 4, pp. 506–510, 2020.

[3] A.-K. Kaliya-Perumal, J. Kharlukhi, and U. F. Omar, "The second wave of COVID-19: time to think of strategic stockpiles," *Canadian Journal of Public Health*, vol. 111, no. 4, pp. 486-487, 2020.

[4] K. Dietz and D. Schenzle, "Mathematical models for infectious disease statistics," in *A celebration of statistics*, A. C. Atkinson and S. E. Fienberg, Eds., pp. 167–204, Springer, New York, NY, 1985.

[5] N. C. Grassly and C. Fraser, "Mathematical models of infectious disease transmission," *Nature Reviews Microbiology*, vol. 6, no. 6, pp. 477–487, 2008.

[6] M. Kretzschmar and J. Wallinga, "Mathematical models in infectious disease epidemiology," in *Modern Infectious Disease Epidemiology*, pp. 209–221, Springer, 2009.

[7] A. Alahmadi, S. Belet, A. Black et al., "Influencing public health policy with data-informed mathematical models of infectious diseases: recent developments and new challenges," *Epidemics*, vol. 32, article 100393, 2020.

[8] A. Krämer, M. Kretzschmar, and K. Krickeberg, *Modern Infectious Disease Epidemiology: Concepts, Methods, Mathematical Models, and Public Health.*, Springer, 2010.

[9] V. Isham and G. Medley, *Models for Infectious Human Diseases: Their Structure and Relation to Data*, vol. 6, Cambridge University Press, 2010.

[10] Mintodê Nicodème Atchadé and Yves Morel Sokadjo, "Overview and cross-validation of COVID-19 forecasting univariate models," *Alexandria Engineering Journal*, vol. 61, no. 4, pp. 3021–3036, 2022.

[11] B. Seidu, C. S. Bornaa, and O. D. Makinde, "An ebola model with hyper-susceptibility," *Chaos, Solitons & Fractals*, vol. 138, article 109938,, 2020.

[12] J. K. K. Asamoah, Z. Jin, G. Q. Sun et al., "Sensitivity assessment and optimal economic evaluation of a new COVID-19 compartmental epidemic model with control interventions," *Chaos, Solitons & Fractals*, vol. 146, p. 110885, 2021.

[13] Z. Yang, Z. Zeng, K. Wang et al., "Modified seir and ai prediction of the epidemics trend of COVID-19 in China under public health interventions," *Journal of Thoracic Disease*, vol. 12, no. 3, pp. 165–174, 2020.

[14] M. Zuo, S. K. Khosa, Z. Ahmad, and Z. Almaspoor, "Comparison of COVID-19 pandemic dynamics in Asian countries with statistical modeling," *Computational and Mathematical Methods in Medicine*, vol. 2020, Article ID 4296806, 16 pages, 2020.

[15] T. Götz and P. Heidrich, "Early stage COVID-19 disease dynamics in Germany: models and parameter identification," *Journal of Mathematics in Industry*, vol. 10, no. 1, pp. 1–13, 2020.

[16] S. He, Y. Peng, and K. Sun, "SEIR modeling of the COVID-19 and its dynamics," *Nonlinear Dynamics*, vol. 101, no. 3, pp. 1667–1680, 2020.

[17] Y. Gu, S. Ullah, M. A. Khan, M. Y. Alshahrani, M. Abohassan, and M. B. Riaz, "Mathematical modeling and stability analysis of the COVID-19 with quarantine and isolation," *Results in Physics*, vol. 34, article 105284, 2022.

[18] C. S. M. Currie, J. W. Fowler, K. Kotiadis et al., "How simulation modelling can help reduce the impact of COVID-19," *Journal of Simulation*, vol. 14, no. 2, pp. 83–97, 2020.

[19] G. Huang, Q. Pan, S. Zhao, Y. Gao, and X. Gao, "Prediction of COVID-19 outbreak in China and optimal return date for university students based on propagation dynamics," *Journal of Shanghai Jiaotong University (Science)*, vol. 25, no. 2, pp. 140–146, 2020.

[20] A. Senapati, S. Rana, T. Das, and J. Chattopadhyay, "Impact of intervention on the spread of COVID-19 in India: a model based study," 2020, https://arxiv.org/abs/2004.04950.

[21] T. Zhou, Q. Liu, Z. Yang et al., "Preliminary prediction of the basic reproduction number of the Wuhan novel coronavirus 2019-nCoV," *Journal of Evidence-Based Medicine*, vol. 13, no. 1, pp. 3–7, 2020.

[22] Y. Fang, Y. Nie, and M. Penny, "Transmission dynamics of the COVID-19 outbreak and effectiveness of government interventions: a data-driven analysis," *Journal of Medical Virology*, vol. 92, no. 6, pp. 645–659, 2020.

[23] C. Hou, J. Chen, Y. Zhou et al., "The effectiveness of quarantine of Wuhan city against the Corona Virus Disease 2019 (COVID-19): a well-mixed SEIR model analysis," *Journal of Medical Virology*, vol. 92, no. 7, pp. 841–848, 2020.

[24] S. Q. Du and W. Yuan, "Mathematical modeling of interaction between innate and adaptive immune responses in COVID-19 and implications for viral pathogenesis," *Journal of Medical Virology*, vol. 92, no. 9, pp. 1615–1628, 2020.

[25] F. Petropoulos and S. Makridakis, "Forecasting the novel coronavirus COVID-19," *PLoS One*, vol. 15, no. 3, article e0231236, 2020.

[26] S. Nana-Kyere, J. Ackora-Prah, E. Okyere, S. Marmah, and T. Afram, "Hepatitis b optimal control model with vertical transmission," *Applications of Mathematics*, vol. 7, no. 1, pp. 5–13, 2017.

[27] B. R. Rowthorn and F. Toxvaerd, *The optimal control of infectious diseases via prevention and treatment, CEPR Discussion Paper No. DP8925*, 2012.

[28] Z. Feng, Y. Yang, and X. Dashun, "Timely identification of optimal control strategies for emerging infectious diseases," *Journal of Theoretical Biology*, vol. 259, no. 1, pp. 165–171, 2009.

[29] A. Di Liddo, "Optimal control and treatment of infectious diseases. The case of huge treatment costs," *Mathematics*, vol. 4, no. 2, p. 21, 2016.

[30] H. Behncke, "Optimal control of deterministic epidemics," *Optimal Control Applications & Methods*, vol. 21, no. 6, pp. 269–285, 2000.

[31] F. Lin, K. Muthuraman, and M. Lawley, "An optimal control theory approach to non-pharmaceutical interventions," *BMC Infectious Diseases*, vol. 10, no. 1, pp. 1–13, 2010.

[32] E. F. Arruda, S. S. Das, C. M. Dias, and D. H. Pastore, "Modelling and optimal control of multi strain epidemics, with application to COVID-19," *PLoS One*, vol. 16, no. 9, article e0257512, 2021.

[33] G. B. Libotte, F. S. Lobato, and G. M. P. A. J. Silva Neto, "Determination of an optimal control strategy for vaccine administration in COVID-19 pandemic treatment," *Computer*

Methods and Programs in Biomedicine, vol. 196, article 105664, 2020.

[34] S. Nana-Kyere, E. Okyere, and J. D.-G. Ankamah, "Compartmental seirw COVID-19 optimal control model," *Communications in Mathematical Biology and Neuroscience*, vol. 2020, 2020.

[35] J. K. K. Asamoah, M. A. Owusu, Z. Jin, F. T. Oduro, A. Abidemi, and E. O. Gyasi, "Global stability and cost-effectiveness analysis of COVID-19 considering the impact of the environment: using data from Ghana," *Chaos, Solitons & Fractals*, vol. 140, article 110103, 2020.

[36] C. Tsay, F. Lejarza, M. A. Stadtherr, and M. Baldea, "Modeling, state estimation, and optimal control for the us COVID-19 outbreak," *Scientific Reports*, vol. 10, no. 1, pp. 1–12, 2020.

[37] A. Kouidere, B. Khajji, A. El Bhih, O. Balatif, and M. Rachik, "A mathematical modeling with optimal control strategy of transmission of COVID-19 pandemic virus," *Communications in Mathematical Biology and Neuroscienc*, vol. 2020, 2020.

[38] T. Alex Perkins and G. España, "Optimal control of the COVID-19 pandemic with non-pharmaceutical interventions," *Bulletin of Mathematical Biology*, vol. 82, no. 9, pp. 1–24, 2020.

[39] Chernet Tuge Deressa and Gemechis File Duressa, "Modeling and optimal control analysis of transmission dynamics of COVID-19: the case of Ethiopia," *Alexandria Engineering Journal*, vol. 60, no. 1, pp. 719–732, 2021.

[40] A. K. Srivastav, M. Ghosh, X.-Z. Li, and L. Cai, "Modeling and optimal control analysis of COVID-19: case studies from Italy and Spain," *Mathematical Methods in the Applied Sciences*, vol. 44, no. 11, pp. 9210–9223, 2021.

[41] B. Seidu, "Optimal strategies for control of COVID-19: a mathematical perspective," *Scientifica*, vol. 2020, Article ID 4676274, 12 pages, 2020.

[42] S. Nana-Kyere, F. A. Boateng, P. Jonathan et al., "Global analysis and optimal control model of COVID-19," *Computational and Mathematical Methods in Medicine*, vol. 2022, Article ID 9491847, 20 pages, 2022.

[43] O. Agossou, "Mintodê Nicodème Atchadé and Aliou Moussa Djibril. "Modeling the effects of preventive measures and vaccination on the COVID-19 spread in benin republic with optimal control"," *Results in Physics*, vol. 31, article 104969, 2021.

[44] M. A. Khan, A. Atangana, E. Alzahrani, and Fatmawati, "The dynamics of COVID-19 with quarantined and isolation," *Advances in Difference Equations*, vol. 2020, Article ID 109953, 425 pages, 2020.

[45] C. Castillo-Chavez, Z. Feng, and W. Huang, "On the computation of r 0 and its role on global stability," *IMA Volumes in Mathematics and Its Applications*, vol. 125, pp. 229–250, 2002.

[46] M. Y. Li and J. S. Muldowney, "A geometric approach to global-stability problems," *SIAM Journal on Mathematical Analysis*, vol. 27, no. 4, pp. 1070–1083, 1996.

[47] A. Khan, R. Zarin, G. Hussain, N. A. Ahmad, M. H. Mohd, and A. Yusuf, "Stability analysis and optimal control of covid-19 with convex incidence rate in Khyber Pakhtunkhawa (Pakistan)," *Results in Physics*, vol. 20, article 103703, 2021.

[48] R. H. Martin Jr, "Logarithmic norms and projections applied to linear differential systems," *Journal of Mathematical Analysis and Applications*, vol. 45, no. 2, pp. 432–454, 1974.

[49] J. K. Asamoah, F. Nyabadza, Z. Jin et al., "Backward bifurcation and sensitivity analysis for bacterial meningitis transmission dynamics with a nonlinear recovery rate," *Chaos, Solitons & Fractals*, vol. 140, article 110237, 2020.

[50] A. M. Niger and A. B. Gumel, "Mathematical analysis of the role of repeated exposure on malaria transmission dynamics," *Differential Equations and Dynamical Systems*, vol. 16, no. 3, pp. 251–287, 2008.

[51] F. Brauer, "Backward bifurcations in simple vaccination models," *Journal of Mathematical Analysis and Applications*, vol. 298, no. 2, pp. 418–431, 2004.

[52] H. Abboubakar, J. C. Kamgang, and D. Tieudjo, "Backward bifurcation and control in transmission dynamics of arboviral diseases," *Mathematical Biosciences*, vol. 278, pp. 100–129, 2016.

[53] M. Tilahun, "Backward bifurcation in sirs malaria model," 2017, https://arxiv.org/abs/1707.00924.

[54] C. Castillo-Chavez and B. Song, "Dynamical models of tuberculosis and their applications," *Mathematical Biosciences and Engineering*, vol. 1, no. 2, pp. 361–404, 2004.

[55] N. Chitnis, J. M. Hyman, and J. M. Cushing, "Determining important parameters in the spread of malaria through the sensitivity analysis of a mathematical model," *Bulletin of Mathematical Biology*, vol. 70, no. 5, pp. 1272–1296, 2008.

[56] H. S. Rodrigues, M. Teresa, T. Monteiro, and D. F. M. Torres, "Sensitivity analysis in a dengue epidemiological model," *Conference Papers in Science*, vol. 2013, Article ID 721406, 7 pages, 2013.

[57] R. E. Kopp, "Pontryagin maximum principle," *Mathematics in Science and Engineering*, vol. 5, pp. 255–279, 1962.

[58] W. H. Fleming and R. W. Rishel, *Deterministic and Stochastic Optimal Control*, Springer Science & Business Media, 2012.

[59] S. Lenhart and J. T. Workman, *Optimal Control Applied to Biological Models*, Chapman and Hall/CRC, 2007.

[60] B. Seidu, O. D. Makinde, and I. Y. Seini, "Mathematical analysis of the effects of HIV-malaria co-infection on workplace productivity," *Acta Biotheoretica*, vol. 63, no. 2, pp. 151–182, 2015.

[61] J. K. Asamoah, Z. Jin, and G. Q. Sun, "Non-seasonal and seasonal relapse model for q fever disease with comprehensive cost-effectiveness analysis," *Results in Physics*, vol. 22, article 103889, 2021.

[62] K.-C. Yang, H.-F. Hung, M.-K. Chen et al., "Cost-effectiveness analysis of universal influenza vaccination: application of the susceptible-infectious-complication-recovery model," *International Journal of Infectious Diseases*, vol. 73, pp. 102–108, 2018.

[63] R. U. Varier, E. Biltaji, K. J. Smith et al., "Cost-effectiveness analysis of treatment strategies for initial _Clostridium difficile infection," *Clinical Microbiology and Infection*, vol. 20, no. 12, pp. 1343–1351, 2014.

[64] B. H. Foy, B. Wahl, K. Mehta, A. Shet, G. I. Menon, and C. Britto, "Comparing COVID-19 vaccine allocation strategies in India: a mathematical modelling study," *International Journal of Infectious Diseases*, vol. 103, pp. 431–438, 2021.

[65] K. Liu and Y. Lou, "Optimizing COVID-19 vaccination programs during vaccine shortages," *Infectious Disease Modelling*, vol. 7, no. 1, pp. 286–298, 2022.

[66] E. Aruffo, P. Yuan, Y. Tan et al., "Mathematical modelling of vaccination rollout and npis lifting on COVID-19 transmission with voc: a case study in Toronto, Canada," *BMC Public Health*, vol. 22, no. 1, pp. 1–12, 2022.

[67] J. Mondal and S. Khajanchi, "Mathematical modeling and optimal intervention strategies of the COVID-19 outbreak," *Nonlinear Dynamics*, vol. 2020, pp. 1–26, 2022.

[68] S. Moore, E. M. Hill, M. J. Tildesley, L. Dyson, and M. J. Keeling, "Vaccination and non-pharmaceutical interventions for COVID-19: a mathematical modelling study," *The Lancet Infectious Diseases*, vol. 21, no. 6, pp. 793–802, 2021.